PKA catalytic subunit β (Cβ) modulates C9orf72-derived dipeptide repeat proteins expression

Nausicaa V Licata[1,2], Riccardo Cristofani[3], Vito G D'Agostino[1,4], Daniele Pollini[1], Rosa Loffredo[1], Michael Pancher[5], Valentina Adami[5], Paola Bellosta[6], Antonia Ratti[7,8], Gabriella Viero[9], Alessandro Quattrone[2], Angelo Poletti[3]* & Alessandro Provenzani[1]*

1 Laboratory of Genomic Screening, Department of Cellular, Computational and Integrative Biology, University of Trento, Trento, Italy;
2 Laboratory of Translational Genomics, Department of Cellular, Computational and Integrative Biology, University of Trento, Trento, Italy;
3 Laboratorio di Biologia Applicata, Dipartimento di Scienze Farmacologiche e Biomolecolari, Università degli Studi di Milano, Milan, Italy;
4 Laboratory of Biotechnology and Nanomedicine, Department of Cellular, Computational and Integrative Biology, University of Trento, Trento, Italy;
5 HTS Core Facility, Department of Cellular, Computational and Integrative Biology, University of Trento, Trento, Italy;
6 Laboratory of Metabolism of Cell Growth and Neuronal Survival, Department of Cellular, Computational and Integrative Biology, University of Trento, Trento, Italy;
7 Istituto Auxologico Italiano, IRCCS, Department of Neurology-Stroke Unit and Laboratory of Neuroscience, Milan, Italy
8 Dipartimento di Biotecnologie Mediche e Medicina Traslazionale, Università degli Studi di Milano, Milan, Italy
9 Institute of Biophysics, CNR Unit at Trento, Trento, Italy

* Corresponding authors: angelo.poletti@unimi.it, alessandro.provenzani@unitn.it

ABSTRACT

The intronic hexanucleotide repeat expansion, *GGGGCC* (*G4C2*), in the *C9orf72* gene is the most common genetic cause of Amyotrophic Lateral Sclerosis (ALS) and Frontotemporal Dementia (FTD) (C9ALS/FTD). The repeat-containing isoforms undergo Repeat-associated non-AUG (RAN) translation producing toxic dipeptide-repeat (DPR) proteins that contribute to neurodegeneration. We developed a high-throughput drug screening to identify positive and negative modulators of DPRs levels. Two hits, Spironolactone and Geldanamycin reduced DPRs expression levels triggering the protein clearance system *in vitro*. Moreover, our screening identified that cAMP-elevating compounds increased DPRs expression levels. Conversely, the PKA inhibitor, H89, reduced DPRs expression levels *in vitro*. H89, in *Drosophila* carrying the G4C2X36 repeats, rescued climbing ability and increased life span of flies. Genetic ablation of the catalytic subunit β (Cβ) of PKA also reduced DPRs expression levels by decreasing their translation efficiency *in vitro* and rescued the pathological phenotype *in vivo*. Together, our results show that protein clearance and PKA-Cβ as new drug targets for C9ALS/FTD, and, in this view, Spironolactone, Geldanamycin and H89 could serve as tool compounds to develop new effective drugs.

INTRODUCTION

Repeat-associated non-AUG (RAN) translation is an unconventional translation associated to several nucleotide-repeated expansions disorders. The hexanucleotide repeat expansion $GGGGCC_n$ (also known as $G4C2_n$) is localized in the first intron of the *C9orf72* gene[1,2] and it is known to be the most common genetic cause of both ALS and FTD (hereafter C9ALS/FTD)[3]. The pathomechanisms proposed for C9ALS/FTD neurodegeneration suggest that the sense and anti-sense $(G4C2)_n$- or $(C4G2)_n$-containing transcripts originate two different mechanisms of toxicity i) by the alteration of RNA processing due to binding and sequestration of RNA-binding proteins, thereby leading to impairment of RNA metabolism[4–12]; and ii) by their unconventional RAN translation into five different dipeptide-repeats (DPRs)[13–15]. In addition, pathological expansion of (G4C2) reduces the *C9orf72* transcription causing loss of function of the C9orf72 protein[1,2]. The toxicity of some of these DPRs has been showed in several cell lines, in iPSC-derived neurons[16–20], in *Drosophila*[10,18,21–23] and in mouse models[24–29]. An impairment of the ubiquitin-proteasome system (UPS) due to aggregation of toxic proteins is largely demonstrated in neurodegenerative disorders and among the mechanisms of DPR-related toxicity. Different studies demonstrated a dysfunction of the UPS due to the sequestration of proteasomal proteins by poly-GA, which arises from frame 1+ of $(G4C2)_n$ transcripts, both *in vitro*[17,19] and *in vivo* models[24]. RAN translation of $(G4C2)_n$-RNAs has been recently shown to require a near-cognate start codon upstream of the repeat in frame +1[30,31] and to be triggered by stress conditions[30,32,33] in a cap-dependent or cap-independent way[30–33]. However, the mechanism regulating RAN translation is still largely unknown. Importantly, no small molecules are known to selectively modulate RAN translation, even if antisense oligonucleotides (ASOs)[34,35] and small molecules binding the $r(GGGGCC)_n$ have been proposed as therapeutics for C9ALS/FTD. Drug screenings identified small molecules targeting the $r(GGGGCC)_n$[16,36,37] and/or $r(CGG)_n$ RNAs[38–40]. These compounds alter the RNA secondary structures providing the proof of principle that small molecules binding $r(GGGGCC)_n$ can inhibit both RNA foci formation and RAN translation. Moreover, the ribosomal protein subunit 25 (RPS25) was recently identified by genetic screen in yeasts as crucial regulator of RAN translation in different repeat sequence expansions[41], while other modifiers of DPR production were identified by two independent genome-wide CRISPR-Cas9 screenings[42,43]. In addition, Cheng *et al*. showed that RAN translation is strongly inhibited by high expression of RNA helicase DDX3X[43].

Here, we used a chemical genomic approach to identify both small molecules and relative molecular targets that can modulate the DPR levels by either increasing protein clearance or inhibiting RAN translation. Among the identified hits, we associated the mechanism of action of two small molecules, Spironolactone and Geldanamycin, to an increased UPS degradative activity. Conversely, our screening identified that elevating-cAMP compounds increased DPRs expression levels indicating the Adenylyl cyclase/Protein Kinase A (AC/PKA) path as a crucial modulator of the translation process of the *C9orf72* mRNA and suggesting the PKA inhibitor H89 as a blocker of RAN translation.

RESULTS

Development of a HTS assay for identifying modulators of C9orf72-DPRs expression

RAN translation of expanded $(G4C2)_n$ repeats is intrinsically low if compared to the canonical translation due to the absence of an AUG start codon. Initial efforts to set up an assay amenable for high-throughput screening (HTS), were performed using several reporters. We tested either luciferase and GFP reporters downstream of $(G4C2)_{66}$[44] (Supplementary Fig. 1a) or $(G4C2)_{58}$[22] repeat-containing vectors, respectively, and also bicistronic vector having the $(G4C2)_{58}$-GFP downstream of a AUG-RFP-STOP coding sequence (Supplementary Fig. 1c). In transiently transfected SH-SY5Y human neuronal cells, all the reporters showed no measurable levels of RAN products (Supplementary Fig. 1b and 1c). In addition, $(G4C2)_{58}$-GFP signal was generally lost in few generations of stable SH-SY5Y cells, possibly because of the toxicity of the DPR products. We obtained a satisfactory rate of $(G4C2)_{58}$-GFP signal using a reverse transfection approach in HEK293T cells (Supplementary Fig. 1d). To note, the GFP coding sequence was placed in frame +2 (poly-GP) (hereafter polyGP-GFP). Using this strategy, we set up the HTS assay co-transfecting the polyGP-GFP and an AUG-RFP plasmids (Fig. 1a), used as positive control for AUG-mediated translation. Cycloheximide (CHX) was used as positive control to check general translation arrest with respect to untreated cells (negative control). We used the variation in the number of GFP or RFP positive cells as read-out of the assay. In these conditions, the variability and the robustness of the assay were optimized to perform a HTS assuming CHX as positive control for RFP cells (Z factor = 0.5)[45] (Supplementary Fig. 1e). We observed that CHX did not decrease the fluorescence intensity or the number of cells expressing polyGP-GFP (Supplementary Fig. 1f), possibly due to the stability of the DPRs in this time-frame[20].

We screened about 2,500 compounds with biological activity from different chemical libraries (see Material and Methods). Treatments were started 3 h after plasmids co-transfection, GFP and RFP reporter signals were measured 36 h later. Plotting the Z-score of the number of cells expressing CAP-products (RFP, Y axis) *vs* the Z-score of the number of cells expressing DPR-products (polyGP-GFP, X axis), we obtained a graphical representation of the simultaneous effect of the small molecules either on the accumulation of canonical CAP (AUG) translation-dependent or on the RAN translation-dependent products (Fig. 1b). The majority of tested compounds did not modify the expression level of the two fluorescent reporters, indirectly proving the quality of assay. We gated effective molecules by excluding the central cloud of non-effective compounds, using an arbitrary threshold of cells expressing polyGP-GFP ±1.5 and ±1 for AUG-derived positive cells. The highly toxic compounds were excluded using the threshold Z-score nuclei ≤-2, indicating that the number of surviving cells accounted for less than 50%. A confirmatory screening was performed as above, but further increasing the number of replicates from 1 to 4. As expected, only few compounds were able to significantly reduce the RAN products, while many add an opposite effect (Fig. 1c). This comes as no surprise, because the majority of the RAN-increasing compounds were blockers of the degradative pathways (e.g. Thapsigargin, Tunicamycin or MG132). We chose 5 hit compounds according to the ability of specifically decrease or increase the number of cells expressing polyGP-GFP and/or the fluorescence intensity of GFP (Table 1): Spironolactone (SPL), an aldosterone antagonist; Geldanamycin (GA), an inhibitor of Heat Shock Protein 90 (HSP90); Forskolin (FSK), a cAMP-elevating compound which acts as a direct stimulator of the Adenylyl Cyclase (AC) enzyme. We also included two phytochemicals, Erysolin (ERY) and Helenin (HLN), with undefined mechanism of action. Interestingly, FSK, by activating AC and enhancing intracellular cAMP levels, triggers a multitude of PKA-dependent and/or –independent pathways resulting in pleiotropic effects into the cells. These events include the activation of many intracellular signalling cascades and of the cAMP Response Elements Binding (CREB) family of transcription factors that, upon phosphorylation, regulates the expression level of genes containing CREs in their promoters[46–48]. We then performed dose-response experiments by treating cells with two concentration ranges of the selected compounds (Fig. 1d and 1e), checking their toxicity and the effects on DPR expression. All the compounds confirmed their activity to modulate the number of polyGP-GFP positive cells, although to various extent. The most potent one was FSK that selectively increased polyGP-GFP positive cells compared to AUG-RFP positive cells. HLN decreased both products, while ERY, GA and SPL decreased more efficiently the polyGP-GFP products than the AUG-RFP. All these compounds were moderately toxic at concentrations higher than 40 μM, being HLN the most toxic one. Therefore, we excluded HLN due to its toxicity and prosecuted with SPL, GA, ERY and FSK to gain information about their molecular mechanism of action.

Geldanamycin and Spironolactone induce degradation of DPRs by enhancing the UPS

We first investigated whether the 4 selected DPR modulators (Fig. 2a) affected transcription and translation. To this aim, we used the incorporation of the modified nucleoside 5-ethynyl uridine (EU) to evaluate general RNA transcription and of the O-propargyl-puromycin (OPP) to evaluate *de-novo* protein synthesis. GA marginally induced general transcription (Fig. 2b), but none of the compounds had an effect on translation (Fig. 2c). The molecular mechanism of RAN translation initiation is still matter of debate and a CUG start codon within the first intron has been suggested to play a key the role in *C9orf72* gene RAN translation[31]. To further evaluate whether the effect of these compounds was CUG independent, we used a construct containing 66 repeats[44] that also includes the endogenous near-cognate CUG codon in a perfect Kozak sequence, 24 nucleotides upstream of the repeat and in frame with poly-GA (+1)[31]. GA and SPL reduced the accumulation of poly-GA (HA-tagged) also in the presence of the upstream CUG (Fig. 2d and 2e). To prove the efficacy of GA and SPL in motoneuronal derived cells, we used the immortalized mouse cell line NSC34 (Supplementary Fig. 2a). GA and SPL significantly reduced both the soluble levels and the PBS-insoluble species of poly-GP in NSC34 cells (Fig. 2f, g and h). FSK significantly increased both poly-GA (Fig. 2d, and 2e) and the PBS insoluble species of poly-GP (Fig. 2f, 2g and 2h) in NSC34 cells. In contrast, ERY did not show any effect in modulating the PBS insoluble species of poly-GP (Fig. 2f, 2g and 2h). The modulation of DPR expression was not dependent on different amount of *G4C2* mRNA (Supplementary Fig. 2b and 2c). Among the possible post-transcriptional/post-translational mechanisms underlying modulatory effect of our selected small molecules, we investigated their activity on DPR clearance. DPRs mainly rely upon autophagy for their degradation, while, in basal condition, only polyGP is degraded by the UPS[19,49,50]. However, dysfunctions in protein quality control machinery have been largely demonstrated in ALS, C9ALS/FTD as well as in other neurodegenerative disorders[17,19,51]. Therefore, we evaluated the expression level of autophagy markers (p62/SQSTM1, LC3, HSPB8, BAG3) using as positive control the natural compound trehalose[52]. None of the compounds induced neither the protein expression (Fig. 3a and 3b) nor the transcripts level of autophagy markers in NSC34 (Fig. 3c) or in SH-SY5Y (Supplementary Fig. 3a) cells. Immunofluorescence analysis also showed that p62/SQSTM1 and LC3 intracellular distribution were not modified by the treatment with the various compounds in NSC34 cells (Supplementary Fig. 3b and 3c). These data ruled out a role of autophagy in the mechanism of action of our hits. To investigate a possible involvement of the UPS in DPRs degradation, we transfected cells with a GFP construct tagged with a short degron (CL1) (GFPu) that directs the reporter protein to the proteasome for its degradation[49,53]; thus, UPS impairment correlates with GFPu accumulation. We found that both GA and SPL increased the functionality of the UPS to degrade the reporter GFPu, while ERY did not, FSK led to a marked GFPu accumulation into both NSC34 (Fig. 3d) and SH-SY5Y (Supplementary Fig. 3d) cells. Contrary to expectations[54,55], GFPu accumulation by FSK was not due to a block in the UPS, as CHX chase experiment indicated that the degradation kinetic was identical between FSK and control condition (Supplementary Fig. 4a and 4b). In addition, we did not observe an increase of *GFPu* mRNA (Supplementary Fig. 4c, 4d and 4e). Collectively, these data suggest that GA and SPL reduce the level of DPRs by enhancing the function of the UPS pathway, without interfering with the autophagy machinery. However, we cannot exclude further mechanisms of action, at present. Conversely, ERY does not reduce the DPR-derived insoluble material nor trigger the UPS. Interestingly, the effect of these compounds was not either cell type-dependent or CUG-dependent. FSK did not have an effect on inhibiting the UPS and, given the known molecular target of FSK, we decided to further investigate on the mechanism of action elicited by this molecule.

PKA inhibition decreases DPRs expression without affecting degradative pathways

FSK is a derivative of the geranylgeranyl pyrophosphate (GGPP), characterized by the insertion of an heterocyclic ring of tetrahydropyran-derivated[56], and differs from the analogous geranylgeranyl acetone (GGA), which is a potent inducer of HSP70, HSPB8 and HSPB1[57,58] (thus a modulator of the protein quality control system and autophagy). As an internal additional validation of the screening results, we observed that other compounds that increase cAMP (e.i. Dibutyryl cAMP·Na, Desacetylcolforsin, Colforsin and Cilostazol) were all able to increase the amount of DPRs within HEK293T cells

(Supplementary Fig. 5a). To prove the importance of the AC/PKA pathway in increasing the RAN product, we re-tested Cilostazol (CLZ), a phosphodiesterase III (PDE III) inhibitor that increases cAMP level by reducing its degradation, and tested the PKA inhibitor, H89 (Fig. 4a). Notably, in HEK293T cells, 10 µM of CLZ showed an effect similar to FSK, while 2.5 µM of H89 reduced poly-GA (Fig.4b and c). As suggested by the co-administration of FSK and H89, the increase of RAN products, by the cAMP stimulation, was blocked by H89. This result suggests the importance of PKA, more than of cAMP, in determining the accumulation of DPRs (Fig.4b and 4c). The same results were obtained in NSC34 cells, in which poly-GP expression and PBS insoluble fractions were decreased following 2.5 µM treatment with H89, and the increase of FSK was dampened by H89 (Fig. 4d, 4e and 4f). H89 slightly reduced the mRNA expression level of RAN transcripts (Supplementary Fig. 5b and 5c) and did not induce an autophagic response, as it did not modulate SQSTM1/p62 or LC3 levels in both NSC34 (Supplementary Fig. 5d, 5f, 5g, 5h and 5i) and SH-SY5Y cells (Supplementary Fig. 5e). Moreover, H89 did not induce the degradation of the GFPu reporter containing the CL1 degron, supporting that FSK and H89 may exert their effect via a mechanism, which does not involve protein degradation by the UPS (Supplementary Fig. 5j and 5k).

PKA inhibition decreases DPRs expression modulating *G4C2* mRNA translation.

We then focused on examining whether PKA was fundamental in modulating the expression of DPRs. H89 is defined as a specific PKA inhibitor, but when used at concentration ≥ 10 µM, it loses specificity showing some PKA-independent activities and the interpretation of the cellular effects may become uncertain[59–62]. Indeed, H89 reduces the phosphorylation of PKA substrates in a dose dependent manner (Supplementary Fig. 5l), and it loses its PKA-specificity at high doses, also becoming toxic (IC50 20 µM on HEK293T cells) (Supplementary Fig. 5m). Therefore, to assess whether PKA played a role in modulating the expression of DPRs, PKA expression was silenced. In humans, *PRKACA* and *PRKACB* are two genes encoding for the PKA catalytic subunits α (Cα) and β (Cβ), respectively. Using RNA interference, we genetically ablated the expression of both the Cα and the Cβ subunits. We found that a marked reduction of Cα expression (42%) slightly decreased the level of poly-GA (26.4%) (Fig. 5a, 5b and 5c). In contrast, the low reduction of Cβ expression (23%) significantly reduced the level of poly-GA (37.4%) (Fig. 5d, 5e and 5f). However, while we observed a marked reduction of *PRKACA* mRNA upon *PRKACB* silencing (Supplementary Fig. 6a), we did not observe the contrary under silencing of *PRKACA* gene (Supplementary Fig. 6b), suggesting a stronger inhibition of PKA activity during *PRKACB* silencing. Next, we checked whether the total expression level of *G4C2* transcripts was changed during the silencing of *PRKACA* and *PRKACB*. We found that in both conditions the total level of *G4C2* transcripts was not changed (Supplementary Fig. 6c). Therefore, we reasoned whether PKA could act at the translational level and checked the polysomal loading of *G4C2* RNA under either silencing of *PRKACA* or *PRKACB*. Surprisingly, we found that ablation of *PRKACA* slightly shifted *G4C2* RNA from heavy to light polysomes (Fig. 5g upper inset), compared to the control condition, while the silencing of *PRKACB* strongly repressed the translation of *G4C2* transcript (Fig. 5h upper inset). On the other hand, the silencing of *PRKACB* marginally changed the polysomal loading of *GAPDH* mRNA (Fig. 5h lower inset), and the silencing of *PRKACA* showed a non-significant change of polysomal loading on *GAPDH* mRNA (Fig. 5g lower inset). Despite these changes, we did not observe any significant change in *de-novo* protein synthesis under the silencing of *PRAKCA* and *PRKACB* (Supplementary Fig. 6d, 6e, 6f and 6g). Collectively, these data demonstrate that PKA effectively plays a role in modulating DPRs level, without affecting the degradation of DPRs, but by affecting the translatability of the aberrantly expanded *G4C2* mRNA sequence.

PKA inhibition rescues motility defects and animal survival in *Drosophila* model for C9ALS/FTD.

To assess *in vivo* the effect of PKA inhibition, we used a *Drosophila* model for C9ALS/FTD expressing a sequence of 36 G4C2 repeats of the *C9orf72* gene in neurons using the *elav-Gal4* driver [21]. These transgenic flies show a reduction in lifespan[21] and a progressive loss of motility (Fig 6a and 6c). Therefore, *Elav-C9orf72-G4C2* adults were treated daily from 1 day after eclosion (DAE) with 10µM H89 and their ability to climb was tested every two days[63]. H89 significantly improved the motility of the flies carrying the repeats starting from the 3 DAE, while did not show any significant effect in *wild type elav-w*^{1118} flies (Fig. 6a, 6c). *Elav-C9orf2-G4C2* female flies showed a significant improvement in their climbing activity with a 50% of success that increased in the presence of H89 from 7 to 10 days DAE, while in *elav-/w1118* control females the treatment with H89 did not show any significant effect (Fig. 6a). In males the ability of H89 to ameliorate the motility of *elav-C9orf72-G4C2* animals was also significant but with a less extend (*p<0.05) than in females (***p<0.001) flies (Fig. 6c). Moreover, H89 increased the viability in both female and male *elav-C9orf72-G4C2* flies compared to the mutants treated with negative control (Fig. 6b, 6d), suggesting a beneficial effect also on animal survival. To further prove the

PKA relevance in mediating the expansion toxicity, we genetically reduced in neurons the level of *Pka-C1* (*Pka-C1*, that is the *PRKACB* human homolog), using an *UAS-RNAi* line against the catalytic subunit of PKA in combination with the expression of *UAS-C9orf72*-G4C2. (Supplementary Fig. 7a). The data clearly demonstrated that the downregulation of Pka-C1 significantly ameliorated both motility defects (Fig. 7a and 7c) and lethality (Fig. 7b and 7d) in adult female and male flies expressing *C9orf72*-G4C2 strongly indicating the relevance of PKA in mediating the toxicity of the *C9orf72*-G4C2 expansion.

DISCUSSION

We performed a chemical screening by using libraries of small molecules with known molecular mechanism of action and used the expression level of polyGP-GFP as readout. Contrary to other efforts[43], we were not able to obtain cell clones stably overexpressing the polyGP-GFP products. However, we succeeded in the optimization of a robust assay that allowed the identification of a number of small molecules that modulated the expression level of the RAN products. Among the internal controls, we could observe that blockers of general translation, as mTOR inhibitors (e.g. Torin, Rapamycin) and ribosome targeting antibiotics (as Puromycin), were able to decrease the expression level of both RAN- and AUG-dependent products. Also using genetic deconvolution, we identified 3 small molecules of which 2, SPL and GA decreased the overall level of DPRs, while in contrast FSK markedly increased DPR levels. SPL is an aldosterone antagonist that targets the Mineralcorticoid Receptor (MR). Its antihypertensive effect was thought to depend primarily on its diuretic and saluretic action. However, it appears that part of its mechanism of action is due to the blockade of the MR in other tissues than the kidneys as the cardiac tissue and the CNS[64]. Indeed, SPL is able to induce ubiquitin-activating enzyme and proteasome mediated degradation of the helicase xeroderma pigmentosum group B complementing protein (XPB), independent of its MR blocking effect, in HeLA cells[65] and in human pulmonary artery endothelial cells (PAECs)[66]. Moreover, it is known that SPL with its diuretic effect, can act on Na^{+} and Ca^{2+} metabolism and it has been shown that SPL was able to increase the survival rate of flies carrying CUG-repeat expansions suppressing their semi-lethal phenotypes[67]. Given the ability of SPL to cross the blood brain barrier[64], its activity should be evaluated in *in vivo* model to reduce the formation of RAN products into neurons. Notably, SPL is a commercially available drug, used as oral suspension to aid patients with difficult swallowing including ALS patients. Therefore, it might be interesting to evaluate whether C9orf72-ALS patients may have benefit in disease progression after SPL treatment, compared to non-treated patients. GA is the “first in class” discovered HSP90 inhibitor[68]. GA inhibits HSP90 binding to its amino terminus impeding its binding to misfolded proteins, thereby inducing their proteasomal degradation[69]. Since many of these clients are oncogenic proteins, the antitumoral effect of GA is due to the degradation of these oncodrivers[70]. Unfortunately, no HSP90 inhibitors have been approved for clinical usage, even if a number of HSP90 inhibitors, including some GA derivatives like 17-AAG and 17-DMAG, are presently in advanced phase II clinical trial for a variety of cancers. Their clinical utilization is based on their capability to induce the heat shock response (HSR), a pro-survival response that upregulates the expression of the protective-stress induced small HSP, like HSPB1 and HSP70[71–73] that is, however, detrimental for the anticancer therapy. HSPB1, like its cognate HSPB8[49,50], show protective effects by inducing proteasome or autophagic degradation of ubiquitinated and misfolded proteins[73]. A plausible explanation of our data is that RAN products can be clients of the HSP90 protein and that GA inhibits the stabilization effect of the HSP90, by also triggering the HSR and enhances the DPRs UPS-mediated clearance in cells, as already shown in previous study by our group[50]. To note, the activation of the UPS by SPL and GA, triggered the degradation of poly-GA that is not normally degraded via this mechanism[50].

Our screening also identified FSK as a potent inducer of polyGP-GFP expression levels. FSK acts as stimulator of the AC enzyme thereby increasing intracellular cAMP levels and regulating several downstream pathways by activation of PKA[47,48]. We examinated that the PKA inhibitor, H89, decreased RAN products expression in different cell models and improved motor dysfunction and survival rates in *Drosophila* model for C9ALS/FTD, showing a generality in the mechanism of action. We also noted a potential gender related effects in C9orf72-related effects[74] but this may also be explained by the dosage compensation effect of the *X* chromosome[75] where the *elav-Gal4* transgene is inserted. H89 is thought to inhibit PKA by competitively binding the ATP site on its catalytic subunit[76]. However, several studies demonstrated that H89 shows effects that are PKA independent. To provide evidences of the involvement of PKA in our model, we then silenced its catalytic subunits *in vitro* and *in vivo* with the simultaneous expression of the *G4C2-C9orf72* expansion. Depletion of Cβ showed a marked reduction of poly-GA protein expression more than the silencing of Cα, but no changes in *G4C2* mRNA expression were observed. In addition, the silencing of *PRAKCB* also entailed a reduced *PRKACA* mRNA expression, but not conversely. Moreover, ablation of *PRKACB* strongly repressed the translation of G4C2 transcripts *in vitro* and ablation of its homolog *Pka-C1* in neurons of *Drosophila* significantly ameliorated both motility defects and lethality in flies carrying *C9orf72*-G4C2. Of note, Cβ is more specifically expressed in neuronal tissue[77,78] than Cα, and depletion of *PRKACB* in mice resulted to be protective by age-related effects[79]. Interestingly, there are evidences that PKA is involved in the regulation of translation at different levels. In fungi, PKA is involved in regulating the translation by: i) activation of de-capping enzymes Dcp1/2, via Pat1 (deadenylation factor) phosphorylation, thereby allowing the association of the translational machinery to mRNA and protecting it from degradation and ii) regulation of the abundance of eIF4G[80,81]. Moreover, PKA has been reported to regulate translation elongation by phosphorylating the eEF2 kinase (eEF2K), which in turn phosphorylates eEF2, thereby slowing down the elongation phase[82]. An intriguing hypothesis is that PKA-Cβ regulates translation of specific genes and the mechanism of *G4C2* mRNA regulation is dependent on the translation mechanism driven by the specific activation of PKA. Finally, we obtained a strong rescue of motility and enhanced survival of the affected flies using either H89 or the conditional knockout of PKA in the nervous tissue, suggesting PKA-Cβ as a novel target for ALS due to G4C2 expanded *C9orf72*. A plausible hypothesis explaining the selective involvement of PKA in mediating the neuronal toxicity of the G4C2 expansion could be related to the cross-talk between the neuronal excitatory signalling, leading to cAMP formation that activates the PKA pathway(s). For example, the calcium-permeable AMPA (CP-AMPA) receptors are normally expressed at low levels at the synapses and its expression on the synapse surface requires the phosphorylation of GluA1 serine 845 by PKA[83]. Interestingly, it has been showed that the increase of intracellular oligomeric amyloid β promotes the synaptic expression of CP-AMPA in a PKA- and CAMKII-dependent way[84], even if how it occurred remains undefined. Therefore, given the involvement of PKA in mediating different signalling pathways at the neuronal tissues, it is important further elucidating its potential role in C9ALS/FTD and in other neurodegenerative diseases characterized by repeat expansion. To note, FSK is largely sold as a dietary supplement to aid in weight loss and muscle building, but, according to these data, it could lead to serious, long term, adverse events and additional studies should be taken before consumption. In summary, in this work, we identified 3 small molecules, SPL, GA and indirectly H89 that reduced the DPRs content. From one side, we found SPL and GA act by enhancing the function of the UPS, suggesting that targeting degradative machinery may represent a valid therapeutic approach to decrease the C9ALS/FTD disease progression. To the other side, with FSK and H89 we identified that the AC/PKA-Cβ pathway regulates the expression level of RAN products at the translational level, grounding the work for further exploration of new molecular targets for *G4C2* expanded in *C9ALS/FTD*.

Acknowledgements: We thank Prof. Leonard Petrucelli (Mayo Clinic, Jacksonville, FL, USA) kindly provided G4C2x2 or x66 plasmids, prof. Taylor (St. Jude Children's Research Hospital, Memphis, TN, USA) kindly provided G4C2x58 or x8 plasmids, Prof. Anna Cereseto (University of Trento, Trento, Italy) kindly provided AUG-RFP plasmid, Prof. Ron Kopito (Stanford University, Stanford, CA, USA) kindly provided the GFPu proteasome reporter. We thank the Bloomington *Drosophila* Stock Center and the VDRC StockCenter for fly lines. This work was supported by grants from: Fondazione Cassa di Risparmio di Trento e Rovereto (Drug repositioning project #40102838) to AlP and AQ; Fondazione ARISLA (project TARGET RAN # 40103385 to AlP and AnP and project MLOpathy to AnP); Fondazione Cariplo, Italy (n. 2014-0686, # 40102636) to AnP; Fondazione Telethon, Italy (GGP19128 to AnP); Kennedy's disease association (2018 grant to RC); Italian Ministry of University and Research (MIUR); PRIN - Progetti di ricerca di interesse nazionale (n. 2017F2A2C5 to AnP); Agenzia Italiana del Farmaco (AIFA) (Co_ALS to AnP); Fondazione Regionale per la Ricerca Biomedica (FRRB) (Regione Lombardia, TRANS_ALS, project nr. 2015-0023, to AnP).

Author contributions: AnP (unimi) and AlP (unitn). designed research; NVL, RC, AR, VGD, AQ, PB, GV, AnP (unimi) and AlP (unitn) analyzed the data; NCV, RC, VGD, DP, RL, MP, VA, PB and GV performed research; NVL, RC prepared the figures; NVL, AnP (unimi) and AlP (unitn) wrote the manuscript with input from all authors.

Conflict of Interest: The authors declare they are filing a patent to protect the utilization of spironolactone as therapeutic agent to treat C9ALS/FTD

ORCID

Nausicaa Valentina Licata http://orcid.org/0000-0003-0750-0692

Riccardo Cristofani http://orcid.org/0000-0003-2719-846X

Vito Giuseppe D'Agostino https://orcid.org/0000-0003-3379-2254

Daniele Pollini https://orcid.org/0000-0001-7782-7960

Rosa Loffredo https://orcid.org/0000-0001-7981-9227

Michael Pancher https://orcid.org/0000-0002-3783-6069

Valentina Adami https://orcid.org/0000-0002-0617-9393
Paola Bellosta https://orcid.org/0000-0003-1913-5661
Antonia Ratti https://orcid.org/0000-0002-4264-6614
Gabriella Viero https://orcid.org/0000-0002-6755-285X
Alessandro Quattrone https://orcid.org/0000-0003-3333-7630
Angelo Poletti http://orcid.org/0000-0002-8883-0468
Alessandro Provenzani https://orcid.org/0000-0003-1652-3415

Materials and Methods

Chemicals

The chemicals utilized in this study are the following: Geldanamycin (GA; InvivoGen, ant-gl), Erysolin (ERY; Santa Cruz Biotechnology, sc-205679), Spironolactone (SPL; Santa Cruz Biotechnology, sc-204294), Forskolin (FSK; SelleckChem, S2449), Cilostazol (CLZ; Cayman Chemical, 15035), H-89 hydrochloride (H89; Cayman Chemical, 10010556), Cycloheximide (CHX; Sigma-Aldrich, C1988), ActinomycinD (ACTD; Sigma-Aldrich, A9400), Dimethyl sulfoxide (DMSO; Sigma-Aldrich, 41639), Trehalose (TREH, Sigma-Aldrich, T9531).

The primary screening was conducted using the following compound libraries: i) the Spectrum Collection library (MicroSource, USA) containing 60% of FDA/EMA-approved drugs, 25% of natural products and 15% of molecules in preclinical stages for a total of 2000 compounds; ii) the Anti-cancer compound library (Selleck), a unique collection of 349 bioactive compounds; iii) the NIH Clinical Collection assembled by the National Institutes of Health (NIH) comprised of 450 molecules that have a history of use in human clinical trials; iv) the Screen-Well® Autophagy library (Enzo Life Science) containing 94 compounds with defined autophagy-inducing or -inhibitory activity.

Cell cultures and transfections

The human embryo kidney HEK293T cell line was cultured in standard conditions using in Dulbecco's modified Eagle's medium (DMEM) (Sigma-Aldrich) with 10% FBS (Sigma-Aldrich), 1% L-glutamine (Sigma-Aldrich) and 1% penicillin–streptomycin (Sigma-Aldrich). HEK293T cells were plated at $1x10^5$ or 5 $x10^4$ cells per well (for siRNA experiments) in 12-well plates for RT-qPCR and immunoblotting, $1.2x10^4$ or $2.5x10^3$ per well (for siRNA experiments) in 96-well plates for viability cell assay and dose-response assay, $1.2x10^4$ cells per well in 384-cell plates for primary and secondary screenings. The immortalized motoneuronal cell line NSC34[85,86], cultured in standard condition using DMEM (Euroclone) with 5% FBS (Sigma-Aldrich), 1 mM L-glutamine (EuroClone) and antibiotics (penicillin, SERVA; streptomycin, SERVA). NSC34 cells were plated at $8x10^4$ cells per well in 12-well plates for RT-qPCR, immublotting and FRA analyses. SH-SY5Y human neuroblastoma cell line was cultured in DMEM/F12 (EuroClone) supplemented with 10% FBS (Sigma-Aldrich), 1mM L-glutamine (EuroClone) and antibiotics (penicillin, SERVA; streptomycin, SERVA). SH-SY5Y cells were plated at $1.5x10^5$ cells per well in 12-well plates for RT-qPCR and immunoblotting. Plasmid and siRNA transfections were performed using

Lipofectamine 3000 (Invitrogen) and Opti-MEM (Thermo Scientific) following the manufacturer's instructions. Plasmid transfections in 384-well plates were performed using the reverse protocol.

Plasmids and siRNAs

The pcDNA3.1-CMV-GGGGCCx58-GFP vector was kindly provided by prof. Taylor[87] (St. Jude Children's Research Hospital, Memphis, TN, USA). Plasmids were fully confirmed by sequencing. The pAG3-CAG-GGGGCCx2 or GGGGCCx66 (2R or 66R) vectors with three epitope tags per frame were kindly provided by Prof. Leonard Petrucelli[44] (Mayo Clinic, Jacksonville, FL, USA). Nanoluc-containing recombinant plasmids were obtained using the pAG3-2R and pAG3-66R vector backbones. The sequence of the nanoluc was sub-cloned from pNL1 vector (Promega), after PCR amplification, using the unique NotI restriction site present in the vector upstream of the FLAG/HA/Myc tags. The AUG-RFP vector was kindly provided by Prof. Anna Cereseto[88] (University of Trento, Trento, Italy). pcDNA3.1-CMV-GGGGCCx58-GFP and AUG-RFP were utilized to perform the primary and secondary screening and dose-response assay. The plasmid expressing the proteasome reporter GFPu was kindly provided by Prof. Ron Kopito[53] (Stanford University, Stanford, CA, USA). The pCMV-β (Clontech) and pSV-β-gal (Promega) plasmids encoding for β-galactosidase. The plasmid pcDNA3.1 (ThermoFisher) has been used to normalize the total DNA amount in each transfection.

To silence endogenous human *PKA catalytic* isoforms we used siRNAs targeting *PKA catalytic subunit α* (esiRNA human PRKACA, EHU132541) and *PKA catalytic subunit β* (esiRNA human PRKACB, EHU075621) purchased from Sigma-Aldrich.

High-throughput and confirmatory screening

The screening protocol used in this study was the following:

Day 1: reverse transfection, cell seeding and treatment with compound-libraries

1.1 reverse transfection

Human HEK293T cells were seeded into the wells contained pre-aliquoted transfection mixture consisting of 25ng G4C2x58-GFP and 25ng AUG-RFP. To allow the complete addiction of the transfection mixture into the well (2.5 µL per well), it was diluted 5 times with OptiMen, adding so 12.5 µL per well. The transfection mixture was automatically transferred from a 96 well plate to a 384 well plate (CellCarrier-384 Ultra microplates, Perkin Elmer, #6057300) by Tecan Freedom EVO 200 liquid handler.

1.2 cells seeding

HEK293T cells were cultured in T75 cm2 flaks (Corning®) until to 85-90% of confluence. Cells were trypsinized for 30 sec in order to avoid aggregates and re-suspended to a concentration of $3.2x10^5$ cells/mL in DMEM. By Tecan Freedom EVO 200 liquid handler, 37.5 µL of cells were dispensed into each well (containing 12.5 µL of transfection mix) in order to get a final density of $1.2x10^4$ cells per well in 50 µL tot. Plates were spun down briefly and then incubated at 37°C and 5% CO_2 for 3 h.

1.3 cells treatment with compound-libraries

Compound-libraries were added after that cells adhesion to the well bottom (3 h). The compounds were automatically added with Tecan Freedom EVO 200 liquid handler at the final concentrations of 5 µM in one replicate well. Cycloheximide was used as positive control at a final concentration of 5 µM, while the vehicle DMSO, at a final concentration of 0.5% was used as negative control. Plates were spun down briefly and then incubated at 37°C and 5% CO_2 for 36 h.

Day 2: cell imaging and analysis

Cells were imaged after an incubation of 30 min with Hoechst 33342, added by an automated multidispenser (BioTek EL406). Optimized steps gain a GFP S/N higher than 1.5 and a RFP S/N higher than 5 for the negative controls. Image acquisition was performed using an Operetta High-Content Imaging System (Perkin Elmer). Three channels were acquired: Hoechst33342 Ex 380/40nm, Em 445/70nm; GFP Ex 475/30nm, Em 525/50nm; RFP Ex 535/30nm, Em 595/70nm. Two fields of view were acquired for each well (representing 33% of the entire well) using a 10x Objective 0.4NA. Image analysis was performed using Harmony 4.1 software (Perkin Elmer). Quickly, cell number was estimated counting Hoechst positive nuclei and the transfection rate cells was defined as GFP or RFP positive cells. Hits were defined as compounds capable to selectively reduce or increase the number of cells polyGP-GFP positive and their fluorescence intensity.

Cell viability assay

In vitro drug sensitivity was assessed in HEK293T cells by the fluorescent and colorimetric OZBlue CellViability kit (OZbiosciences). HEK293T cells were plated $1.2x10^4$ in 96-well plates and treated for 24 h with different concentrations of compounds (and DMSO as negative control) or plated $2.5x10^3$ in 96-well plates for the silencing (72 h) experiments. 8 µL OZBlue Cell Viability Kit was added to the media and incubated for 3 h. Fluorescence measuring (560nm Ex/590nm Em) was determined using a plate reading at the following time-point 1 h, 2 h and 3 h.

The 3-(4,5-dimethyl-2-thiazolyl)-2,5 diphenyl-2H-tetrazolium bromide (MTT; Sigma-Aldrich)-based cell proliferation assay (MTT assay) was carried out on NSC34 cells 24 h with selected compounds, and performed in 24-well plates at 40,000 cells/well (6 wells for each condition to be tested; n = 6). MTT solution was prepared at 1.5 mg/mL in DMEM without phenol red and was filtered through a 0.2-mm filter. Then, the culture medium was removed from the plate and 300 mL of MTT solution was added into each well. Cells were incubated for 30 min at 37°C with 5% CO_2, 95% air and complete humidity. After 30 min, 500 μL of 2-propanol was added into each well and the precipitates were suspended. The optical density (OD) of the wells was determined using a plate reader at a wavelength of 550 nm.

Dose-Response assay

HEK293T cells (1.2x10^4/well in 96-well plates) were co-transfected with poly-GP-GFP and AUG-RFP, treated with different concentrations of compounds for 24 h and Heochst 33342 was added to the living cells for nuclear staining. Image acquisition was performed using an Operetta High-Content Imaging System (Perkin Elmer). 3 channels were acquired: Hoechst33342 Ex 380/40nm, Em 445/70nm; GFP Ex 475/30nm, Em 525/50nm; RFP Ex 535/30nm, Em 595/70nm. Image analysis was performed using Harmony 4.1 software (Perkin Elmer). Cell number was estimated counting the nuclei Hoechst positive and the transfected cells was defined as GFP or RFP positive cells. Hits were defined as compounds capable to selectively reduce or increase the number of cells RAN-GFP positive and the GFP fluorescence intensity.

RNA and protein click-iT imaging kits

Click-iT RNA Alexa Fluor 488 Imaging Kit (Thermo Scientific) was used to quantify the level of global RNA synthesis by imaging. HEK293T cells were treated for 24 h with compounds (or DMSO) and for 3 h with 5 μM ActD (used as positive control of inhibitor of RNA synthesis), and then incubated for 1 h with 1 mM 5-ethynyl uridine (EU) working solution without removing the drug-containing media. EU detection was performed following the manufacturer’s protocol after cell fixation and permeabilization by imaging. Heochst 33342 was used for DNA staining.

Click-iT Plus OPP Alexa Fluor 488 Protein Synthesis Assay Kit (Thermo Scientific) was used to measure the rate of translation. HEK293T cells were treated for 24 h with compounds (or DMSO) and for 3 h with 350 μM CHX (used as positive control to inhibit translation), and then incubated for 30 min with 20 μM O-propargyl-puromycin (OPP) in working solution without removing the drug-containing media. After fixation and permeabilization, OPP incorporation was assessed by imaging. NuclearMask Blue Stain was used for DNA staining and Operetta acquisition and analysis.

RT-qPCR

HEK293T cells were seeded in 12-well plates. Transfection with 66R was performed 24 h after and treatments immediately after transfection. Cells were harvested 24 h after treatments and centrifuged 5 min at 1200 rpm at 4°C; pellets were re-suspended in 300 mL of TRI Reagent (Thermo Scientific) and total RNA isolated according to manufacturer's instructions. RNA quantification was carried out by absorbance at 260 nm.

The retrotranscription reaction was performed starting from 1 μg of RNA using the RevertAid First Strand cDNA synthesis kit (Thermo Scientific) according to the manufacturer's protocol using 0.5 μL random primers and 0.5 μL Oligo(dT) primers (Invitrogen). qPCR was carried out using the CFX Connect Real-Time PCR Detection System (BioRad) using Kapa Syber Fast qPCR Mastermix (Kapa Biosystems).

The primers used for the qPCR are listed in Supplementary Table 2. Relative mRNA quantification was obtained with the ΔCt method using *Gapdh* as housekeeping gene. Relative mRNA quantification of *G4C2* was obtained by normalizing for the amount of transfected plasmid.

NSC34 and SH-SY5Y cells were plated in 12-well plates, allowed to growth for 24 h and then treated with compounds or DMSO (used as negative control). Cells were harvested 24 h after treatments and centrifuged 5 min at 100 X g at 4°C; the pellets were resuspended in 300 mL of TRI Reagent (Sigma-Aldrich) and total RNA isolated according to manufacturer's instructions. RNA quantification was carried out by absorbance at 260 nm. Total RNA (1 μg) was treated with DNAse I (Sigma-Aldrich), and reverse transcribed into cDNA using the High-Capacity cDNA Archive Kit (Life Technologies) according to the manufacturer's protocol. qPCR was carried out using the CFX 96 PCR Detection System (BioRad) using iTaq Universal SYBR® Green Supermix (Biorad). The primers used for the qPCR are listed in Supplementary Table 2. Relative mRNA quantification was obtained with the ΔCt method using *Rplp0*/*RPLP0* as housekeeping genes.

Lysates preparation and immunoblotting

HEK293T cells were plated in 12-well plates (3 wells for each condition to be tested; n = 3). 24 h after plating, cells were transfected with 2R (as negative control) or 66R plasmids and treated immediately after transfection with compounds for 24 h. For the silencing of *PRAKCA* and *PRKACB*, cells were siRNA transfected 24 h after plating and transfected with plasmid 48 h after the siRNA transfection. 24 or 72 h after plating, HEK293T were harvested and centrifuged 5 min at 1,200 rpm at 4°C, then cells were lysed for 15 min in RIPA lysis buffer supplemented with the Protease Inhibitor Cocktail (Sigma-Aldrich). Supernatants were collected after centrifugation at 12,000 rpm for 20 min, and protein concentration was determined using the Bradford method (Sigma-Aldrich). Equal amounts of total proteins extract was separated on 12% or 15% SDS–PAGE gels, transferred onto PVDF membranes (Amersham Hybond, GE Healthcare) and blocked with 5% (v/v) nonfat dried milk powder (EuroClone) in Tris–buffered saline with Tween 20 0.1% (Sigma-Aldrich) (TBS-T; pH 7.5). The membranes were then incubated overnight at 4 °C in TBS-T with 5% (v/v) BSA with one of the primary antibodies (listed in Supplementary Table 1) washed twice with TBS-T, incubated with horseradish peroxidase (HRP)-conjugated secondary antibodies (donkey anti-rabbit GE Healthcare Life Sciences #NA934, sheep anti-mouse GE Healthcare Life Sciences #NA931) and washed with TBS-T. Signal was revealed with chemiluminescence detection kit reagents (Amersham ECL Select, GE Healthcare).

NSC34 or SH-SY5Y cells were plated in 12-well plates (3 wells for each condition to be tested; n = 3). 24 h after plating, cells were transfected as previously described and treated with compounds for 24 h. In experiments involving autophagy induction 100 mM trehalose for the last 48 h were added to the cells. 48 or 72 h after plating, cells were harvested and centrifuged 5 min at 100 X g at 4°C; the cell pellets were resuspended in PBS (Sigma- Aldrich) supplemented with the Protease Inhibitor Cocktail (Sigma-Aldrich) and homogenized using slight sonication to lyse cells and nuclei as previously described[89] . Total proteins were determined with the bicinchoninic acid method (QPRO BCA assay; Cyanagen). Equal amounts of total proteins extract was separated on 10% or 15% SDS–PAGE gels, transferred onto PVDF membranes (polyscreen transfer membrane; Amersham) and blocked with 5% (v/) non-fat dry milk powder (EuroClone) in Tris-buffered saline with 0.1% Tween 20 (TBS-T; pH 7.5). The membranes were then incubated overnight at 4°C with the primary antibodies (listed in Supplementary Table 1), washed twice with TBS-T, incubated with horseradish peroxidase (HRP)-conjugated secondary antibodies (goat anti-rabbit Jackson Immunoresearch Laboratories 111–035-003, goat anti-mouse Jackson Immunoresearch Laboratories 115–035-003). Signal was revealed with chemiluminescence detection kit reagents (WESTAR ANTARES Western ECL Blotting Substrate; Cyanagen, XLS142). Membranes were subsequently processed with different antibodies to detect the levels of different proteins in the same sample, after stripping for 20 min at room temperature (Renew Stripping Buffer, Cyanagen).

Filter retardation assay (FRA)

FRA was performed using a Bio-Dot SF Microfiltration Apparatus (Bio-Rad). 8 µg of the total proteins were filtered through a 0.2-µm cellulose acetate membrane (Whatman). Slot-blots were probed as described for immunoblotting. ChemiDoc XRS System (Bio-Rad, Hercules, California, USA) was used for the image acquisition of FRA. Optical density of samples assayed with FRA was detected and analysed using the Image Lab software (Bio-Rad). Statistical analyses have been performed using the relative optical densities defined as the ratio between optical densities of each independent biological sample ($n = 3$) and the mean optical density.

Immunostaining and Confocal Microscope Analysis

NSC34 cells were seeded on coverslips at a density of $3x10^4$ cells per well (in 24-well plates), and the day after plating were transfected and/or treated with compounds. After treatments, cells were fixed at 37°C for 25min using a solution 1:1 of 4% paraformaldehyde (Sigma-Aldrich) in PB 0.2 M [solution made of KH_2PO_4 (0.06 M) and Na_2HPO_4 (0.26 M)] and 4% (v/v) sucrose (Sigma-Aldrich) in PB 0.2 M. Then, fixing solution was removed and cold methanol was added for 10min to complete the fixation. Cell permeabilization was performed using a solution of 0.2% TRITON X100 (Sigma-Aldrich) followed by incubation for 1 h in blocking solution. Incubation with the primary antibody was kept over-night at 4°C. Incubation with the fluorescent-tagged secondary antibody was preceded by three washes with PBS, to remove the excess of primary antibody. Nuclei were stained with DAPI (Sigma-Aldrich). The primary antibodies used are listed in Supplementary Table 1.The following secondary antibodies were used: goat anti-rabbit Alexa 594 (Thermo Scientific, A-11012; dilution 1:1,000). All the primary and secondary antibodies were diluted in blocking solution (5% nonfat dried milk in 1X PBS-T). Coverslips were mounted on a glass support using MOWIOL and images were acquired using Eclipse Ti2 (Nikon, Netherlands) confocal microscope equipped with A1 plus camera (Nikon) and processed with the NIS-Elements software (Nikon) processed with Fiji ImageJ distribution[90] based on ImageJ version: 2.0.0-rc-69/1.52p.

β-galactosidase assay

NSC34 cells were plated in 24-well plate at density of $4x10^4$ cells/well (6 wells for each condition to be tested; n = 3) and transfected with 0.4 µg of pCMV-βgal or pSV-βgal plasmids. 48 h after transfection, cells were lysed in 250 µL of lysis buffer (Promega) and 100 µL of samples were added to 750 µL of assay buffer (60 mM Na_2HPO_4 40 mM NaH_2PO_4 10 mM KCl, 1 mM $MgSO_4$, pH 7.0), in presence of 4 mg/mL of β-galactosidase substrate o-nitrophenyl-b-D-galactopyraniside (ONPG; Sigma-Aldrich,) and incubated at 37°C until yellow colour appearance. Then, 500 µL of 1 M Na_2CO_3 were added and 200 µL of the final solution were transferred into a 96-well plate and 420-nm absorbance was evaluated using Enspire plate-reader (PerkinElmer).

Polysome profiling

Polysomal profiling was performed according to previously described protocols[91]. Briefly, the cells were seeded in 10 cm dishes, treated with CHX (10µg/mL) for 4 min and then lysed in 300 µL of cold hypotonic lysis buffer [10 mM NaCl, 10 mM $MgCl_2$•$6H_2O$, 10 mM Tris–HCl, pH 7.5, 1% Triton X-100, 0.2 U/µl Ribolock RNase inhibitor (Thermo Scientific), 0.0005 U/µl DNaseI (Thermo Scientific), CHX 10µg/mL and 1 mM dithio-threitol, 1% sodium deoxycholate]. The lysate was centrifuged at 4°C for 5min at 13,000 rpm to pellet cell debris. The cytoplasmic lysates loaded on a linear 10%–40% [w/v] sucrose gradient and centrifuged in a SW41Ti rotor (Beckman) for 1 h 30 min at 39,000 rpm at 4°C in a Beckman Optima Optima XPN-100 Ultracentrifuge. Fractions of 1 mL of volume were then collected monitoring the absorbance at 254 nm with the UA-6 UV/VIS detector (Teledyne Isco).

Extraction of polysomal RNA and RT-qPCR analysis

Polysomal RNAs were isolated from single fractions along sucrose gradient as described in Tebaldi *et al*.[92]. Collected fractions (polysomal and subpolysomal) were incubated with proteinase K (Thermo Scientific) and 1% SDS for 1 h 45 min at 37°C. After acid phenol–chloroform extraction (Ambion) and isopropanol precipitation, polysomal RNA was re-suspended in 20 µL of water and RNA quantification was determined by 260/280 absorbance ratios using NanoDrop 2000 spectrophotometer (Thermo Scientific). The retrotranscription reaction was performed starting from 1 μL of RNA using the RevertAid First Strand cDNA synthesis kit (Thermo Scientific). qPCR was carried out using the CFX Connect Real-Time PCR Detection System (BioRad) using Kapa Syber Fast qPCR Mastermix (Kapa Biosystems). qPCR were run in three biological and three technical replicates. The percentage of each transcript distribution along the profile was obtained using the following formula: $\% [mRNA]_n = [2^{\wedge 40-Ct\ mRNA}]_n / \Sigma_{n=0->12} [2^{\wedge 40-Ct\ mRNA}]_n$ where n is the number of the fraction, %[mRNA]n is the percentage of mRNA of choice in each fraction.

Fly husbandry and lines

Animals were raised at low density, at 25°C, on a standard food medium containing 9 g/L agar (ZN5 B&V, Italy), 75 g/L corn flour, 60 g/L white sugar, 30 g/L brewer yeast (Acros Organic), 50g/L fresh yeast, and 50 ml/L molasses (Biosigma), along with nipagin and propionic acid (Acros Organic). The fly lines were obtained from the Bloomington *Drosophila* Stock Center: p{UAS-GGGGCC.36} attP40 (B58688)[21], and from Vienna Drosophila Research Center *w*^{1118} (v60000) and UAS\Pka-C1-RNAi p{VSH330111} (v330111), *Pka-C1* UniProtKB code P12370.

H89 treatment in *Drosophila*

One day old animals were transferred in a plastic vial (15 animals for each genotype) containing a Whatmann 3MM paper disc imbibed with 200 μL of H89 diluted to 10 μM final concentration in a 5% sucrose solution with 0.1% DMSO or sucrose and DMSO alone.

Motility assays

One day-old animals of each genotype were transferred in a plastic vial without food (15 animals for each genotype), and their ability to climb up the empty vial after a knock-down to the bottom was analyzed, as previously described[63,93] . The number of flies that were able to climb half of the tube in 15 seconds was recorded. The total number of flies alive was counted every day. Values were expressed as percentage of success with respect to the total number of flies in the vial. For each genotype the test was repeated 20 times for each time-point. After the test, adults were transferred in vials with food and vials were changed every two days with exception of the animals used for the treatment with the drug that were transferred in vials containing 200 μL of a 5% sucrose solution with 0.1% DMSO or sucrose and DMSO alone. In the motility assay the number of survived flies was scored over time. The number of survived flies was also scored. Data are represented as a curve of progressive motility impairment. The statistical analysis of variance (one-way ANOVA) was performed using PRISM GraphPad Software (CA). Bars represent the standard deviation (SD). Experiments were repeated at least three times.

RNA extraction from *Drosophila larvae* and RT-qPCR

Total RNAs were isolated, using 1mL TRI Reagent (Thermo Scientific), from larvae (n=5 for each genotype) of the following genotypes: w^{1118} wild-type control and *Actin-Gal4;UAS-Pka-C1-RNAi*. The retrotranscription reaction was performed starting from 1 µg of RNA using the RevertAid First Strand cDNA synthesis kit (Thermo Scientific) according to the manufacturer's protocol. PCR primers were designed as follows: *Pka* 5'-TTCAGTTCCCCTTCCTCGTC -3' (forward), 5'- GAGGTCCAAGTAGTGCAGGT -3' (reverse); *Actin* 5'- CAGATCATGTTCGAGACCTTCAAC -3' (forward), 5'-ACGACCGGAGGCGTACAG -3' (reverse).

Statistical analysis

Values are expressed as mean ± SD or ± SEM of three independent biological experiments conducted in technical triplicates. Student's t-test, 1-way and 2-way ANOVA were employed to determine statistical significance between control and test groups. Values of $*P<0.05$, $**P<0.01$, $***P<0.001$ and $****P<0.0001$ were considered significant. Data were plotted by GraphPad Prism 6 software.

Supplementary Table 1 | List of antibodies

Antibodies	Dilution	Source	Identifier
rabbit anti-HA affinity purified	1:2,000	Bethyl	A190-108A
rabbit monoclonal anti-P-PKA Substrates (RRXS*/T*) (100G7E)	1:1,000	Cell Signaling	9624S
mouse monoclonal anti- PKAα cat (A-2)	1:500	Santa Cruz Biotechnology	sc-28315
rabbit polyclonal anti-PKA beta catalytic subunit	1:500	Abcam	ab94612
rabbit monoclonal anti-GAPDH (D16H11)	1:3,000	Cell Signaling	5174S
mouse monoclonal anti-αTubulin (TU-02)	1:3,000	Santa Cruz Biotechnology	sc-8035
rabbit polyclonal anti-LC3A/B	1:4,000 (WB) 1:500 (IF)	Sigma-Aldrich	L8918
rabbit polyclonal anti-SQSTM1	1:4,000 (WB)	Sigma-Aldrich	P0067
rabbit polyclonal anti-p62/SQSTM1	1:500 (IF)	Abcam	ab91526
rabbit polyclonal anti-poly-GP	1:2,000	Merck	ABN455
mouse monoclonal anti-GFP	1:5,000	Immunological Sciences	MAB-943459
mouse monoclonal anti-αTubulin	1:4,000	Sigma-Aldrich	T6199

Supplementary Table 2. Primer pairs for Real-Time PCR

Human genes		Primer
G4C2	fwd:	TGC GGT TGC GGT GCC T
	rev*[1]:	CTT GTC GTC GTC GTC CT
	rev*[2]:	AGC GTA ATC TGG AAC GT
Prkaca	fwd:	CCA CTA TGC CAT GAA GAT CCT CG
	rev:	CGA GTT TGA CGA GGA ACG GAA AG
Prkacb	fwd:	GCA GTG GAT TGG TGG GCA TTA G
	rev:	ACT GAA GTG GGA TGG GAA TCG G
Nr4a2f	fwd:	CGA CCA AGA CCT GCT TTT TGA
	rev:	CAA GAC CAC CCC ATT GCA A
Gapdh	fwd:	AGA AGG CTG GGG CTC ATT T
	rev:	CAG GAG GCA TTG CTG ATG AT
Map1LC3-B	fwd:	CGT CCT GGA CAA GAC CA
	rev:	CCA TTC ACC AGG AGG AA
Sqstm1	fwd:	AGG GAA CAC AGC AAG CT
	rev:	GCC AAA GTG TCC ATG TTT CA
Hspb8	fwd:	ATA CGT GGA AGT TTC AGG CA
	rev:	TCT CCA AAG GGT GAG TAC GG
Bag3	fwd:	ATG GAC CTG AGC GAT CTC A
	rev:	CAC GGG GAT GGG GAT GTA
Tfeb	fwd:	GCG GCA GAA GAA AGA CAA TC
	rev:	CTG CAT CCT CCG GAT GTA AT
Rplp0	fwd:	GGT GCC ACA CTC CAT CAT CA
	rev:	AGG CCT TGA CCT TTT CAG TAA GT
Murine Genes		**Primer**
MAP1LC3B	fwd:	CAG CAT CCA ACC AAA ATC CC
	rev:	GTT GAC ATG GTC AGG TAC AAG
SQSTM1	fwd:	CCA GAG AGT TCC AGC ACA GA
	rev:	CCG ACT CCA TCT GTT CCT CA
HSPB8	fwd:	AGA GGA GTT GAT GGT GAA GAC C
	rev:	CTG CAG GAA GCT GGA TTT TC
BAG3	fwd:	GGG TGG AGG CAA AAC ACT AA
	rev:	AGA CAG TGC ACA ACC ACA GC
TFEB	fwd:	CAA GGC CAA TGA CCT GGA C
	rev:	AGC TCC CTG GAC TTT TGC AG
RPLP0	fwd:	GTG GGA GCA GAC AAT GTG GG
	rev:	TGC GCA TCA TGG TGT TCT TG
Bacteria Gene		**Primer**
*Ampicillin**[3]	fwd:	ATG CTT TTC TGT GAC TGG TG
	rev:	GCT ATG TGG CGC GGT ATT AT

*[1] Rev primer designed on HA-tag in frame +1,

*[2] Rev primer designed on His-tag in frame +2

*[3] Antibiotic resistance gene for ampicillin was used to normalize the amount of transfected G4C2 vector

References

1. DeJesus-Hernandez, M. *et al.* Expanded GGGGCC hexanucleotide repeat in noncoding region of C9ORF72 causes chromosome 9p-linked FTD and ALS. *Neuron* **72**, 245–56 (2011).
2. Renton, A. E. *et al.* A hexanucleotide repeat expansion in C9ORF72 is the cause of chromosome 9p21-linked ALS-FTD. *Neuron* **72**, 257–68 (2011).
3. Gijselinck, I. *et al.* A C9orf72 promoter repeat expansion in a Flanders-Belgian cohort with disorders of the frontotemporal lobar degeneration-amyotrophic lateral sclerosis spectrum: a gene identification study. *Lancet Neurol.* **11**, 54–65 (2012).
4. Donnelly, C. J. *et al.* RNA toxicity from the ALS/FTD C9ORF72 expansion is mitigated by antisense intervention. *Neuron* **80**, 415–28 (2013).
5. Lee, Y.-B. *et al.* Hexanucleotide repeats in ALS/FTD form length-dependent RNA foci, sequester RNA binding proteins, and are neurotoxic. *Cell Rep.* **5**, 1178–86 (2013).
6. Mori, K. *et al.* hnRNP A3 binds to GGGGCC repeats and is a constituent of p62-positive/TDP43-negative inclusions in the hippocampus of patients with C9orf72 mutations. *Acta Neuropathol.* **125**, 413–423 (2013).
7. Xu, Z. *et al.* Expanded GGGGCC repeat RNA associated with amyotrophic lateral sclerosis and frontotemporal dementia causes neurodegeneration. *Proc. Natl. Acad. Sci. U. S. A.* **110**, 7778–83 (2013).
8. Haeusler, A. R. *et al.* C9orf72 nucleotide repeat structures initiate molecular cascades of disease. *Nature* **507**, 195–200 (2014).
9. Zhang, K. *et al.* The C9orf72 repeat expansion disrupts nucleocytoplasmic transport. *Nature* **525**, 56–61 (2015).
10. Wen, X. *et al.* Antisense proline-arginine RAN dipeptides linked to C9ORF72-ALS/FTD form toxic nuclear aggregates that initiate invitro and invivo neuronal death. *Neuron* **84**, 1213–1225 (2014).
11. Conlon, E. G. *et al.* The C9ORF72 GGGGCC expansion forms RNA G-quadruplex inclusions and sequesters hnRNP H to disrupt splicing in ALS brains. *Elife* **5**, 56–61 (2016).
12. Swinnen, B. *et al.* A zebrafish model for C9orf72 ALS reveals RNA toxicity as a pathogenic mechanism. *Acta Neuropathol.* **135**, 427–443 (2018).
13. Mori, K. *et al.* Bidirectional transcripts of the expanded C9orf72 hexanucleotide repeat are translated into aggregating dipeptide repeat proteins. *Acta Neuropathol.* **126**, 881–893 (2013).
14. Mori, K. *et al.* The C9orf72 repeat is translated into aggregating dipeptide-repeat proteins in FTD/ALS. *Sci. Mag* **339**, 1335–1338 (2013).
15. Ash, P. E. A. *et al.* Unconventional translation of C9ORF72 GGGGCC expansion generates insoluble polypeptides specific to c9FTD/ALS. *Neuron* **77**, 639–46 (2013).
16. Su, Z. *et al.* Discovery of a Biomarker and Lead Small Molecules to Target r(GGGGCC)-Associated Defects in c9FTD/ALS. *Neuron* **83**, 1043–1050 (2014).

17. May, S. *et al.* C9orf72 FTLD/ALS-associated Gly-Ala dipeptide repeat proteins cause neuronal toxicity and Unc119 sequestration. *Acta Neuropathol.* **128**, 485–503 (2014).

18. Yang, D. *et al.* FTD/ALS-associated poly(GR) protein impairs the Notch pathway and is recruited by poly(GA) into cytoplasmic inclusions. *Acta Neuropathol.* **130**, 525–535 (2015).

19. Yamakawa, M. *et al.* Characterization of the dipeptide repeat protein in the molecular pathogenesis of c9FTD/ALS. *Hum. Mol. Genet.* **24**, 1630–1645 (2015).

20. Westergard, T. *et al.* Repeat-associated non-AUG translation in C9orf72-ALS/FTD is driven by neuronal excitation and stress. *EMBO Mol. Med.* e9423 (2019). doi:10.15252/emmm.201809423

21. Mizielinska, S. *et al.* C9orf72 repeat expansions cause neurodegeneration in Drosophila through arginine-rich proteins. *Science* **345**, 1192–1194 (2014).

22. Freibaum, B. D. *et al.* GGGGCC repeat expansion in C9orf72 compromises nucleocytoplasmic transport. *Nature* **525**, 129–33 (2015).

23. Boeynaems, S. *et al.* Drosophila screen connects nuclear transport genes to DPR pathology in c9ALS/FTD. *Sci. Rep.* **6**, 20877 (2016).

24. Zhang, Y.-J. *et al.* C9ORF72 poly(GA) aggregates sequester and impair HR23 and nucleocytoplasmic transport proteins. *Nat. Neurosci.* **19**, 668–677 (2016).

25. Schludi, M. H. *et al.* Spinal poly-GA inclusions in a C9orf72 mouse model trigger motor deficits and inflammation without neuron loss. *Acta Neuropathol.* **134**, 241–254 (2017).

26. Zhang, Y.-J. *et al.* Poly(GR) impairs protein translation and stress granule dynamics in C9orf72-associated frontotemporal dementia and amyotrophic lateral sclerosis. *Nat. Med.* **24**, 1136–1142 (2018).

27. Zhang, Y.-J. *et al.* Heterochromatin anomalies and double-stranded RNA accumulation underlie C9orf72 poly(PR) toxicity. *Science* **363**, (2019).

28. Hao, Z. *et al.* Motor dysfunction and neurodegeneration in a C9orf72 mouse line expressing poly-PR. *Nat. Commun.* **10**, 2906 (2019).

29. Choi, S. Y. *et al.* C9ORF72-ALS/FTD-associated poly(GR) binds Atp5a1 and compromises mitochondrial function in vivo. *Nat. Neurosci.* **22**, 851–862 (2019).

30. Green, K. M. *et al.* RAN translation at C9orf72-associated repeat expansions is selectively enhanced by the integrated stress response. *Nat. Commun.* (2017). doi:10.1038/s41467-017-02200-0

31. Tabet, R. *et al.* CUG initiation and frameshifting enable production of dipeptide repeat proteins from ALS/FTD C9ORF72 transcripts. *Nat. Commun.* **9**, 152 (2018).

32. Cheng, W. *et al.* C9ORF72 GGGGCC repeat-associated non-AUG translation is upregulated by stress through eIF2α phosphorylation. *Nat. Commun.* **9**, (2018).

33. Sonobe, Y. *et al.* Translation of dipeptide repeat proteins from the C9ORF72 expanded repeat is associated with cellular stress. *Neurobiol. Dis.* **116**, 155–165 (2018).

34. Jiang, J. *et al.* Gain of Toxicity from ALS/FTD-Linked Repeat Expansions in C9ORF72 Is Alleviated by Antisense Oligonucleotides Targeting GGGGCC-Containing RNAs. *Neuron* **90**, 535–550 (2016).

35. Gendron, T. F. *et al.* Poly(GP) proteins are a useful pharmacodynamic marker for C9ORF72-associated amyotrophic lateral sclerosis. *Sci. Transl. Med.* **9**, (2017).

36. Wang, Z.-F. *et al.* The Hairpin Form of r(G4C2)exp in c9ALS/FTD Is Repeat-Associated Non-ATG Translated and a Target for Bioactive Small Molecules. *Cell Chem. Biol.* **26**, 179-190.e12 (2019).

37. Simone, R. *et al.* G-quadruplex-binding small molecules ameliorate C9orf72 FTD/ALS pathology in vitro and in vivo. *EMBO Mol. Med.* **10**, (2018).

38. Yang, W.-Y., Wilson, H. D., Velagapudi, S. P. & Disney, M. D. Inhibition of Non-ATG Translational Events in Cells via Covalent Small Molecules Targeting RNA. *J. Am. Chem. Soc.* **137**, 5336–45 (2015).

39. Yang, W. *et al.* Small Molecule Recognition and Tools to Study Modulation of r(CGG). **11**, 2456–2465 (2016).

40. Green, K. M. *et al.* High-throughput screening yields several small-molecule inhibitors of repeat-associated non-AUG translation. *J. Biol. Chem.* **294**, 18624–18638 (2019).

41. Yamada, S. B. *et al.* RPS25 is required for efficient RAN translation of C9orf72 and other neurodegenerative disease-associated nucleotide repeats. *Nat. Neurosci.* **22**, 1383–1388 (2019).

42. Kramer, N. J. *et al.* CRISPR–Cas9 screens in human cells and primary neurons identify modifiers of C9ORF72 dipeptide-repeat-protein toxicity. *Nat. Genet.* **50**, 603–612 (2018).

43. Cheng, W. *et al.* CRISPR-Cas9 Screens Identify the RNA Helicase DDX3X as a Repressor of C9ORF72 (GGGGCC)n Repeat-Associated Non-AUG Translation. *Neuron* **104**, 885-898.e8 (2019).

44. Gendron, T. F. *et al.* Antisense transcripts of the expanded C9ORF72 hexanucleotide repeat form nuclear RNA foci and undergo repeat-associated non-ATG translation in c9FTD/ALS. *Acta Neuropathol.* **126**, 829–44 (2013).

45. Zhang, J.-H., Chung, T. D. Y. & Oldenburg, K. R. A Simple Statistical Parameter for Use in Evaluation and Validation of High Throughput Screening Assays. *J. Biomol. Screen.* **4**, 67–73 (1999).

46. Sapio, L. *et al.* Targeting protein kinase A in cancer therapy: an update. *EXCLI J.* **13**, 843–55 (2014).

47. Seamon, K. B., Padgett, W. & Daly, J. W. Forskolin: unique diterpene activator of adenylate cyclase in membranes and in intact cells. *Proc. Natl. Acad. Sci. U. S. A.* **78**, 3363–7 (1981).

48. Kanne, H., Prasanna, V., Burte, N. & Gujjula, R. Extraction and elemental analysis of Coleus forskohlii extract. *Pharmacognosy Res.* **7**, 237 (2015).

49. Cristofani, R. *et al.* Inhibition of retrograde transport modulates misfolded protein accumulation and clearance in motoneuron diseases. *Autophagy* **13**, 1280–1303

(2017).

50. Cristofani, R. *et al.* The small heat shock protein B8 (HSPB8) efficiently removes aggregating species of dipeptides produced in C9ORF72-related neurodegenerative diseases. *Cell Stress Chaperones* **23**, 1–12 (2018).

51. Zhang, Y.-J. *et al.* Aggregation-prone c9FTD/ALS poly(GA) RAN-translated proteins cause neurotoxicity by inducing ER stress. *Acta Neuropathol.* **128**, 505–524 (2014).

52. Rusmini, P. *et al.* Trehalose induces autophagy via lysosomal-mediated TFEB activation in models of motoneuron degeneration. *Autophagy* **15**, 631–651 (2019).

53. Bence, N. F., Sampat, R. M. & Kopito, R. R. Impairment of the ubiquitin-proteasome system by protein aggregation. *Science* **292**, 1552–5 (2001).

54. Lokireddy, S., Kukushkin, N. V. & Goldberg, A. L. cAMP-induced phosphorylation of 26S proteasomes on Rpn6/PSMD11 enhances their activity and the degradation of misfolded proteins. *Proc. Natl. Acad. Sci. U. S. A.* **112**, E7176-85 (2015).

55. Huang, H., Wang, H. & Figueiredo-Pereira, M. E. Regulating the Ubiquitin/Proteasome Pathway Via cAMP-signaling: Neuroprotective Potential. *Cell Biochem. Biophys.* **67**, 55–66 (2013).

56. Fuse, M. *et al.* Regulation of geranylgeranyl pyrophosphate synthase in the proliferation of rat FRTL-5 cells: involvement of both cAMP-PKA and PI3-AKT pathways. *Biochem. Biophys. Res. Commun.* **315**, 1147–1153 (2004).

57. Hoshino, T. *et al.* Suppression of Alzheimer's Disease-Related Phenotypes by Geranylgeranylacetone in Mice. *PLoS One* **8**, e76306 (2013).

58. Marunouchi, T., Inomata, S., Sanbe, A., Takagi, N. & Tanonaka, K. Protective effect of geranylgeranylacetone via enhanced induction of HSPB1 and HSPB8 in mitochondria of the failing heart following myocardial infarction in rats. *Eur. J. Pharmacol.* **730**, 140–147 (2014).

59. Davies, S. P., Reddy, H., Caivano, M. & Cohen, P. Specificity and mechanism of action of some commonly used protein kinase inhibitors. *Biochem. J.* **351**, 95–105 (2000).

60. Lochner, A. & Moolman, J. A. The Many Faces of H89: A Review. *Cardiovasc. Drug Rev.* **24**, 261–274 (2006).

61. Limbutara, K., Kelleher, A., Yang, C.-R., Raghuram, V. & Knepper, M. A. Phosphorylation Changes in Response to Kinase Inhibitor H89 in PKA-Null Cells. *Sci. Rep.* **9**, 2814 (2019).

62. Murray, A. J. Pharmacological PKA inhibition: all may not be what it seems. *Sci. Signal.* **1**, re4 (2008).

63. Zhang, S., Feany, M. B., Saraswati, S., Littleton, J. T. & Perrimon, N. Inactivation of Drosophila Huntingtin affects long-term adult functioning and the pathogenesis of a Huntington's disease model. *Dis. Model. Mech.* **2**, 247–266 (2009).

64. Gomez-Sanchez, E. P. Third-generation Mineralocorticoid Receptor Antagonists: Why Do We Need a Fourth? *J. Cardiovasc. Pharmacol.* **67**, 26–38 (2016).

65. Alekseev, S. *et al.* A Small Molecule Screen Identifies an Inhibitor of DNA Repair Inducing the Degradation of TFIIH and the Chemosensitization of Tumor Cells to

Platinum. *Chem. Biol.* **21**, 398–407 (2014).

66. Elinoff, J. M. *et al.* Spironolactone-induced degradation of the TFIIH core complex XPB subunit suppresses NF-κB and AP-1 signalling. *Cardiovasc. Res.* **114**, 65–76 (2018).

67. Garcia-Lopez, A. *et al.* Genetic and Chemical Modifiers of a CUG Toxicity Model in Drosophila. *PLoS One* **3**, e1595 (2008).

68. Whitesell, L., Mimnaugh, E. G., De Costa, B., Myers, C. E. & Neckers, L. M. Inhibition of heat shock protein HSP90-pp60v-src heteroprotein complex formation by benzoquinone ansamycins: essential role for stress proteins in oncogenic transformation. *Proc. Natl. Acad. Sci. U. S. A.* **91**, 8324–8 (1994).

69. Ochel, H. J., Eichhorn, K. & Gademann, G. Geldanamycin: the prototype of a class of antitumor drugs targeting the heat shock protein 90 family of molecular chaperones. *Cell Stress Chaperones* **6**, 105–12 (2001).

70. Sidera, K. & Patsavoudi, E. HSP90 inhibitors: current development and potential in cancer therapy. *Recent Pat. Anticancer. Drug Discov.* **9**, 1–20 (2014).

71. Manaenko, A. *et al.* Heat shock protein 70 upregulation by geldanamycin reduces brain injury in a mouse model of intracerebral hemorrhage. *Neurochem. Int.* **57**, 844–850 (2010).

72. Putcha, P. *et al.* Brain-permeable small-molecule inhibitors of Hsp90 prevent alpha-synuclein oligomer formation and rescue alpha-synuclein-induced toxicity. *J. Pharmacol. Exp. Ther.* **332**, 849–57 (2010).

73. Parcellier, A. *et al.* HSP27 is a ubiquitin-binding protein involved in I-kappaBalpha proteasomal degradation. *Mol. Cell. Biol.* **23**, 5790–802 (2003).

74. Vegeto, E. *et al.* The Role of Sex and Sex Hormones in Neurodegenerative Diseases. *Endocr. Rev.* **41**, (2020).

75. Lucchesi, J. C. & Kuroda, M. I. Dosage compensation in Drosophila. *Cold Spring Harb. Perspect. Biol.* **7**, 1–21 (2015).

76. Engh, R. A., Girod, A., Kinzel, V., Huber, R. & Bossemeyer, D. Crystal structures of catalytic subunit of cAMP-dependent protein kinase in complex with isoquinolinesulfonyl protein kinase inhibitors H7, H8, and H89. Structural implications for selectivity. *J. Biol. Chem.* **271**, 26157–64 (1996).

77. Ørstavik, S. *et al.* Identification of novel splice variants of the human catalytic subunit cβ of cAMP-dependent protein kinase. *Eur. J. Biochem.* **268**, 5066–5073 (2001).

78. Kvissel, A.-K. *et al.* Induction of Cβ splice variants and formation of novel forms of protein kinase A type II holoenzymes during retinoic acid-induced differentiation of human NT2 cells. *Cell. Signal.* **16**, 577–587 (2004).

79. Enns, L. C., Pettan-Brewer, C. & Ladiges, W. Protein kinase A is a target for aging and the aging heart. *Aging (Albany. NY).* **2**, 238–243 (2010).

80. Tudisca, V. *et al.* PKA isoforms coordinate mRNA fate during nutrient starvation. *J. Cell Sci.* **125**, 5221–32 (2012).

81. Leipheimer, J., Bloom, A. L. M. & Panepinto, J. C. Protein Kinases at the Intersection of Translation and Virulence. *Front. Cell. Infect. Microbiol.* **9**, 318 (2019).

82. Liu, R. & Proud, C. G. Eukaryotic elongation factor 2 kinase as a drug target in cancer, and in cardiovascular and neurodegenerative diseases. *Acta Pharmacol. Sin.* **37**, 285–294 (2016).

83. He, K. *et al.* Stabilization of Ca2+-permeable AMPA receptors at perisynaptic sites by GluR1-S845 phosphorylation. *Proc. Natl. Acad. Sci. U. S. A.* **106**, 20033–8 (2009).

84. Whitcomb, D. J. *et al.* Intracellular oligomeric amyloid-beta rapidly regulates GluA1 subunit of AMPA receptor in the hippocampus. *Sci. Rep.* **5**, 10934 (2015).

85. Cashman, N. R. *et al.* Neuroblastoma x spinal cord (NSC) hybrid cell lines resemble developing motor neurons. *Dev. Dyn.* **194**, 209–221 (1992).

86. Durham, H. D., Dahrouge, S. & Cashman, N. R. Evaluation of the spinal cord neuron X neuroblastoma hybrid cell line NSC-34 as a model for neurotoxicity testing. *Neurotoxicology* **14**, 387–95 (1993).

87. Freibaum, B. D. *et al.* GGGGCC repeat expansion in C9orf72 compromises nucleocytoplasmic transport. *Nature* **525**, 129–33 (2015).

88. Francis, A. C. *et al.* Second Generation Imaging of Nuclear/Cytoplasmic HIV-1 Complexes. *AIDS Res. Hum. Retroviruses* **30**, 717–726 (2014).

89. Rusmini, P. *et al.* Aggregation and proteasome: the case of elongated polyglutamine aggregation in spinal and bulbar muscular atrophy. *Neurobiol. Aging* **28**, 1099–111 (2007).

90. Schindelin, J. *et al.* Fiji: An open-source platform for biological-image analysis. *Nature Methods* **9**, 676–682 (2012).

91. Bernabò, P. *et al.* In Vivo Translatome Profiling in Spinal Muscular Atrophy Reveals a Role for SMN Protein in Ribosome Biology. *Cell Rep.* **21**, 953–965 (2017).

92. Tebaldi, T. *et al.* Widespread uncoupling between transcriptome and translatome variations after a stimulus in mammalian cells. *BMC Genomics* **13**, 220 (2012).

93. Vernizzi, L. *et al.* Glutamine Synthetase 1 Increases Autophagy Lysosomal Degradation of Mutant Huntingtin Aggregates in Neurons, Ameliorating Motility in a Drosophila Model for Huntington's Disease. *Cells* **9**, 196 (2020).

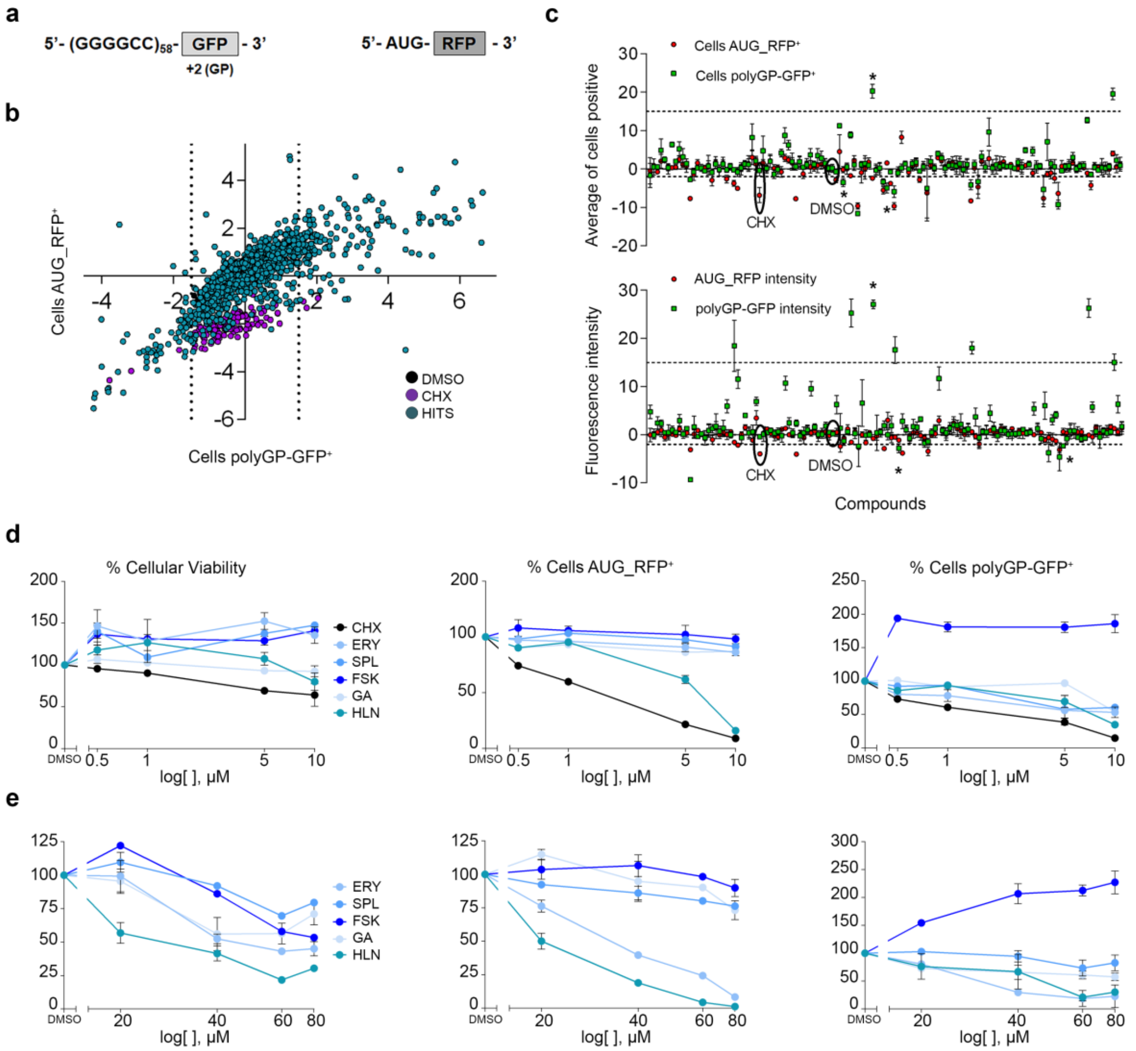

Fig. 1 | High-throughput screening compounds and confirmatory screening for identifying modulators of C9orf72-DPRs expression.

a Schematic representation of the constructs utilized for the screening. The first construct contains 58 G_4C_2 repeats upstream of the GFP, whose AUG was deleted. GFP sequence is in the +2 frame (polyGP-GFP). The second construct contains RFP, whose translation is under the AUG start codon. **b** Primary screening. Scatter plot shows distribution of 2,500 compounds. Y axis represents cells expressing AUG-RFP, while X axis the ones expressing polyGP-GFP. DMSO (black dots) and CHX 5 µM (with dots) were used as negative and positive control, respectively. HEK293T cells were seeded after the addition of transfection mix and incubated at 37°C for 3 h to allow their adhesion to the bottom of the well, then treated with drugs (5 µM). Images and data acquisition were collected after 36 h of treatment. Grid lines represent the threshold set up around DMSO to select effective compounds for the counter-screening and eliminate the ones without any effect. **c** Confirmatory screening. Schematic distributions of cells expressing polyGP-GFP and AUG-RFP (upper inset) and the fluorescence intensity of polyGP-GFP and AUG-RFP relative to each compound (lower inset). * represent small molecules selected. **d** and **e** Dose-response analysis of selected compounds: ERY, SPL, GA, FSK and HLN. Cells were co-transfected with AUG-RFP and polyGP-GFP plasmids and treated with two concentration ranges 0.5, 1, 5 and 10 µM (**d**) and 20, 40 and 60 µM (**e**) for 24 h. Data are mean ± SEM from three biological replicates.

Table 1 | List and Z-score values of hits selected by confirmatory screening

Hit	Cells polyGP-GFP^{+}	Cells AUG-RFP^{+}	polyGP-GFP Fluorescence	AUG-RFP Fluorescence	Cell Viability
Erysolin	-3.5	-0.2	-1.34	-0.7	-1.1
Forskolin	20.3	-2.4	27	-0.8	0.05
Geldanamycin	-5	1.6	0.002	3	-2.6
Helenin	-1.05	-0.7	-2.8	-1.1	-1.3
Spironolactone	-0.5	0.7	-2.3	0.6	-0.9

Mean from 4 biological replicates.

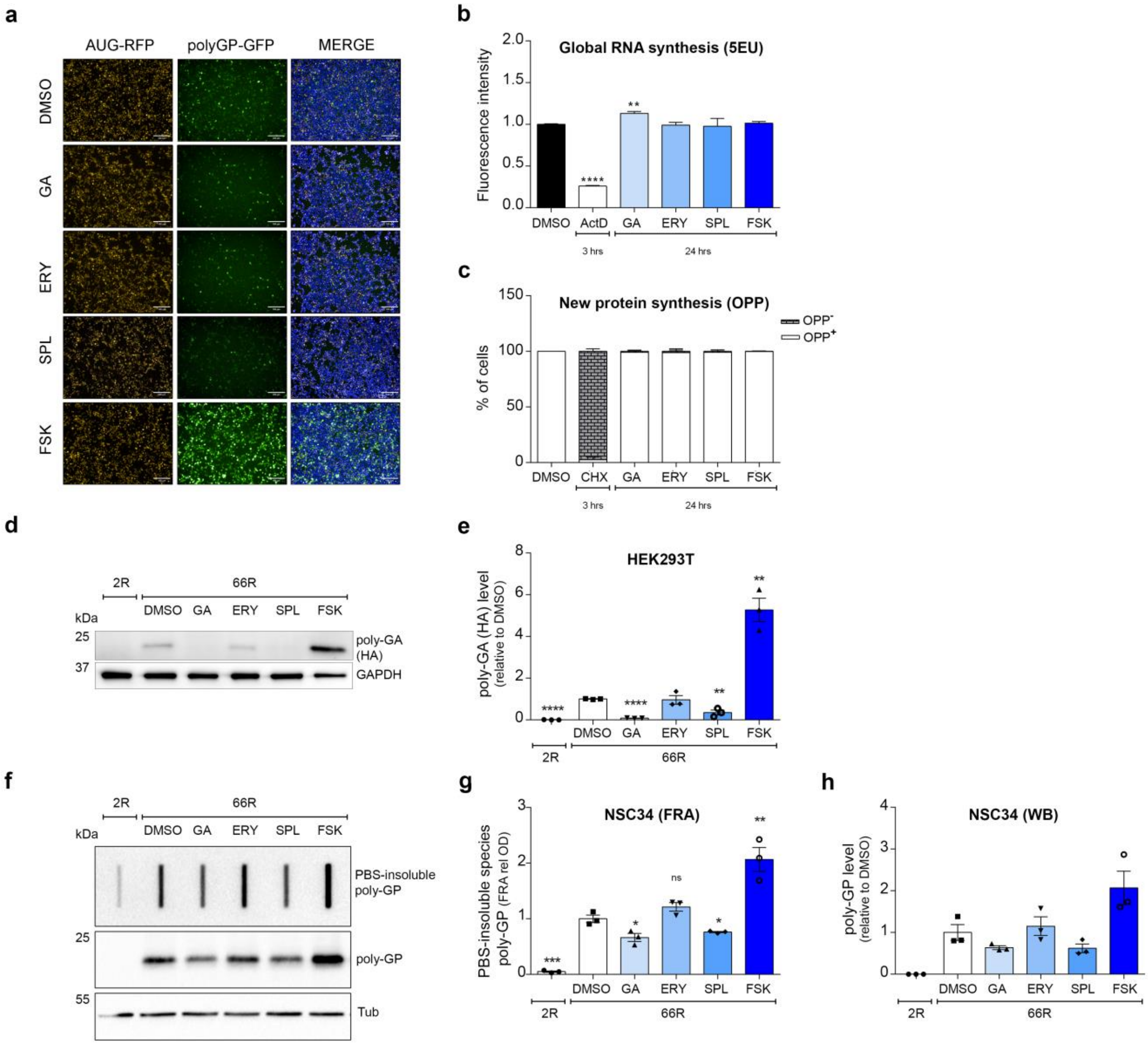
a
AUG-RFP
polyGP-GFP
MERGE
DMSO
GA
ERY
SPL
FSK
b
Global RNA synthesis (5EU)
Fluorescence intensity
DMSO
ActD
GA
ERY
SPL
FSK
3 hrs
24 hrs
c
New protein synthesis (OPP)
% of cells
OPP-
OPP+
DMSO
CHX
GA
ERY
SPL
FSK
3 hrs
24 hrs
d
2R
66R
DMSO
GA
ERY
SPL
FSK
kDa
25
37
poly-GA (HA)
GAPDH
e
HEK293T
poly-GA (HA) level (relative to DMSO)
DMSO
GA
ERY
SPL
FSK
2R
66R
f
2R
66R
DMSO
GA
ERY
SPL
FSK
kDa
PBS-insoluble poly-GP
25
poly-GP
55
Tub
g
NSC34 (FRA)
PBS-insoluble species poly-GP (FRA rel OD)
ns
DMSO
GA
ERY
SPL
FSK
2R
66R
h
NSC34 (WB)
poly-GP level (relative to DMSO)
DMSO
GA
ERY
SPL
FSK
2R
66R

Fig.2 | Effects of hits in different cell lines.

a Images of the HTS representing the effect of the selected small molecules. Scale bar,100 μm**. b** HEK293T cells were treated for 24 h, then general RNA synthesis was monitored using the Click-it chemistry by the incorporation of the nucleoside analogue 5-ethynyl uridine (EU). Actinomycin D 5 μM was used as positive control to block RNA synthesis. Two-tailed, unpaired t-test; ***$P<0.001$, **P 0.0047). **c** Global protein synthesis was monitored as above by the incorporation of the O-propargyl-puromycin (OPP). CHX 350 μM for 3 h was used as positive control to check general translation arrest. **d** Lysates from HEK293T cells, transfected with 2R or 66R and treated with selected compounds for 24 h, immunoblotted using antibodies for poly-GA expression (HA tagged). **e** Quantification of **d** from three biological replicates. Data are mean ± SEM. Two-tailed, unpaired t-test; ****$P<0.0001$, ***$P<0.001$, **P 0.0052 for SPL *versus* DMSO, **P 0.0016 for FSK *versus* DMSO). **f** Lysates from NSC34 cells, transfected with 2R or 66R and treated with selected compounds for 24 h, immunoblotted for insoluble (upper inset) and total soluble (lower inset) poly-GP expression. **g** Quantification of insoluble poly-GP in **f** from three biological replicates. Data are mean ± SEM. Two-tailed, unpaired t-test; ***$P<0.001$, **P 0.0087,*P 0.0256 for GA *versus* DMSO, *P 0.0229 for SPL *versus* DMSO. **h** Quantification of total soluble poly-GP in **f** from three biological replicates. Data are mean ± SEM.

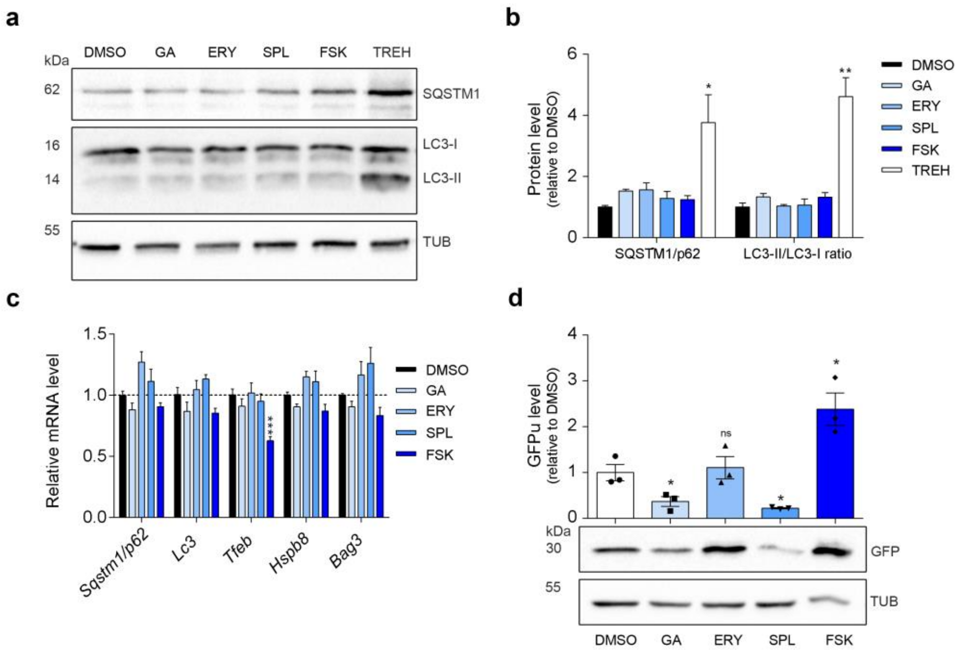

Figure 3 | Geldanamycin and Spironolactone induce degradation of DPRs by enhancing the ubiquitin-proteasome system.

a Lysates from NSC34 cells treated for 24 h and immunoblotted for SQSTM1/p62 and LC3 expression. **b** Quantification of **a** from three biological replicates. Data are mean ± SEM. Two-tailed, unpaired t-test, ***P* 0.0047, **P* 0.0393. **c** Relative expression level of *Sqstm1/p62*, *Lc3*, *Tfeb*, *Hspb8* and *Bag3* mRNAs in NSC34 cells treated for 24 h. Data are mean ± SEM from three biological replicates. 2-way ANOVA followed by Dunnett's multiple comparisons test, **P*>0.05. **d** Lysates from NSC34 cells transfected with a proteasome activity reporter (GFPu), treated for 24 h and immunoblotted for GFP expression. Quantification from three biological replicates. Data are mean ± SEM. Two-tailed, unpaired t-test, **P* 0.0398 GA *versus* DMSO, **P* 0.0124 SPL *versus* DMSO, **P* 0.0253 FSK *versus* DMSO.

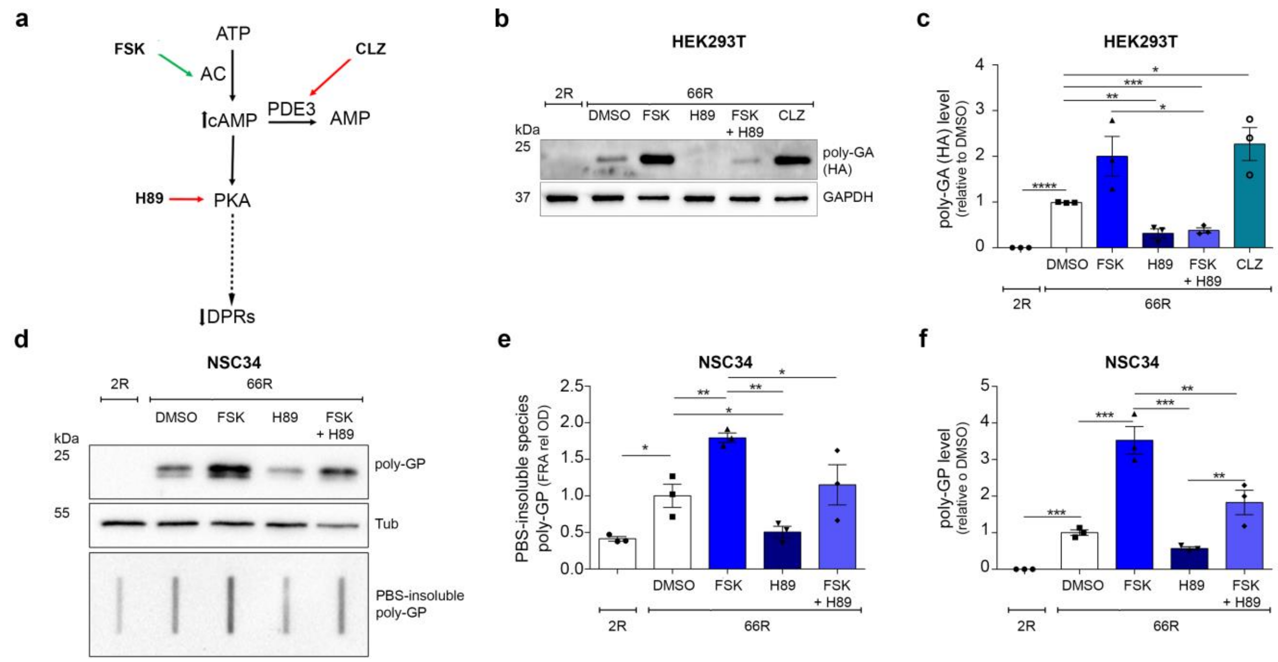

Figure 4 | PKA inhibition decreases DPRs expression levels and modulates G4C2 translation.

a Schematic representation showing where the compounds act along the AC/PKA signalling pathway. **b** Lysates from HEK293T cells, transfected with 2R or 66R and treated with selected compounds for 24 h, immunoblotted using antibody for poly-GA expression (HA–tagged). **c** Quantification of **b** from three biological replicates. Data are mean ± SEM. Two-tailed, unpaired t-test, ****P<0.0001, **P<0.0027 H89 *versus* DMSO, ***P 0.0004 FSK + H89 *versus* DMSO, *P 0.0234 CLZ *versus* DMSO, *P<0.0209 FSK + H89 *versus* FSK. **d** Lysates from NSC34 cells, transfected with 2R or 66R and treated with selected compounds for 24 h, immunoblotted for insoluble (above) and total soluble (below) poly-GP expression. **e** insoluble poly-GP in **d** from three biological replicates. Data are mean ± SEM. 1-way ANOVA followed by uncorrected Fisher's LSD, *P 0.0196 2R *versus* 66R DMSO, **P<0.0039 FSK *versus* DMSO, *P<0.0418 H89 *versus* DMSO, **P 0.0017 H89 *versus* FSK, *P 0.0364 FSK + H89 *versus* FSK. **f** Quantification of total soluble poly-GP in **d** from three biological replicates. Data are mean ± SEM. 1-way ANOVA followed by uncorrected Fisher's LSD, ****P<0.0001 2R *versus* 66R DMSO, ***P 0.0001 FSK *versus* DMSO, ****P<0.0001 H89 *versus* FSK, **P 0.0015 FSK + H89 *versus* FSK, **P 0.0082 H89 *versus* FSK +H89.

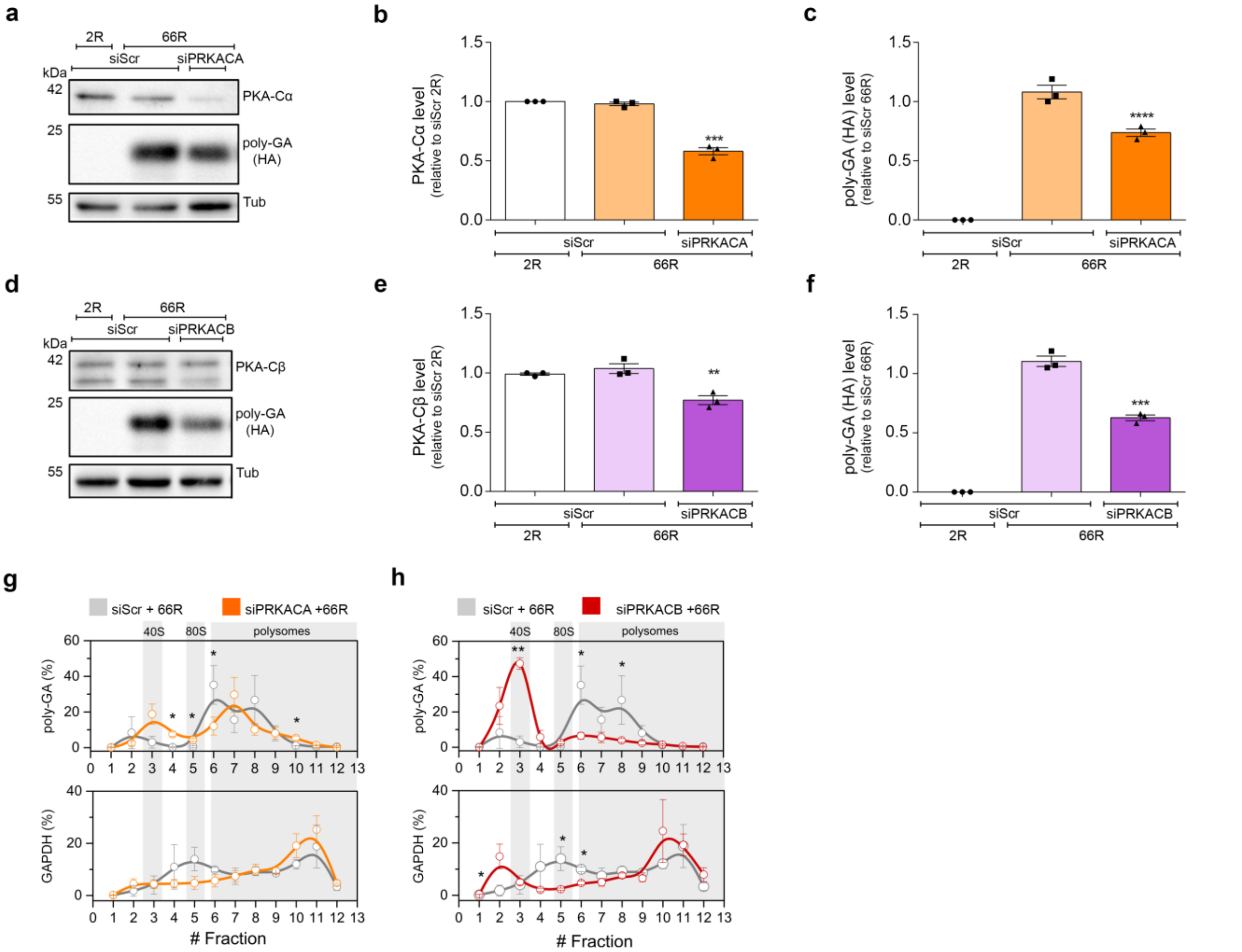

Figure 5 | RNA interference *versus* PKA catalytic subunit β reduces DPRs expression levels by repressing G4C2 translation.

a Lysates from HEK293T cells, transfected with RNAi scramble or RNAi PRKACA (72 h) and with 2R or 66R (24 h), immunoblotted using antibodies for poly-GA (HA tagged) and PRKACB expression. **b** Quantification of PRKACA expression in **a** from three biological replicates. Data are mean ± SEM. Two-tailed, unpaired t-test, ****P* 0.0002 siPRKACA 66R *versus* siScr 66R. **c** Quantification of poly-GA expression in **a** from three biological replicates. Data are mean ± SEM. Two-tailed, unpaired t-test, *****P*<0.0001 siPRKACA 66R *versus* siScr 66R. **d** Lysates from HEK293T cells, transfected with RNAi scramble or RNAi PRKACB (72 h) and with 2R or 66R (24 h), immunoblotted using antibodies for poly-GA (HA tagged) and PRKACB expression. **e** Quantification of PRKACB expression in **d** from three biological replicates. Data are mean ± SEM. Two-tailed, unpaired t-test, ***P* 0.0091 siPRKACB 66R *versus* siScr 66R. **f** Quantification of poly-GA expression in **d** from three biological replicates. Data are mean ± SEM. Two-tailed, unpaired t-test, *****P* 0.0007 siPRKACB 66R *versus* siScr 66R. **g** Co-sedimentation profile of poly-GA (upper panel) and GADPH (lower panel) mRNAs along the sucrose gradient fractions of polysomal profiles from control (grey lines) and PRKACA-depleted (orange lines) cells. Data are mean ± SEM from three independent biological replicates. t-test, one-tailed, *$P < 0.05$; **p-value< 0.01. **h** Co-sedimentation profile of poly-GA (upper panel) and GADPH (lower panel) mRNAs along the sucrose fractions of polysomal profiling from control (grey lines) and PRKACB-depleted (red lines) cells. Data are mean ± SEM from three independent biological replicates. t-test, one-tailed, *$P < 0.05$; **$P < 0.01$.

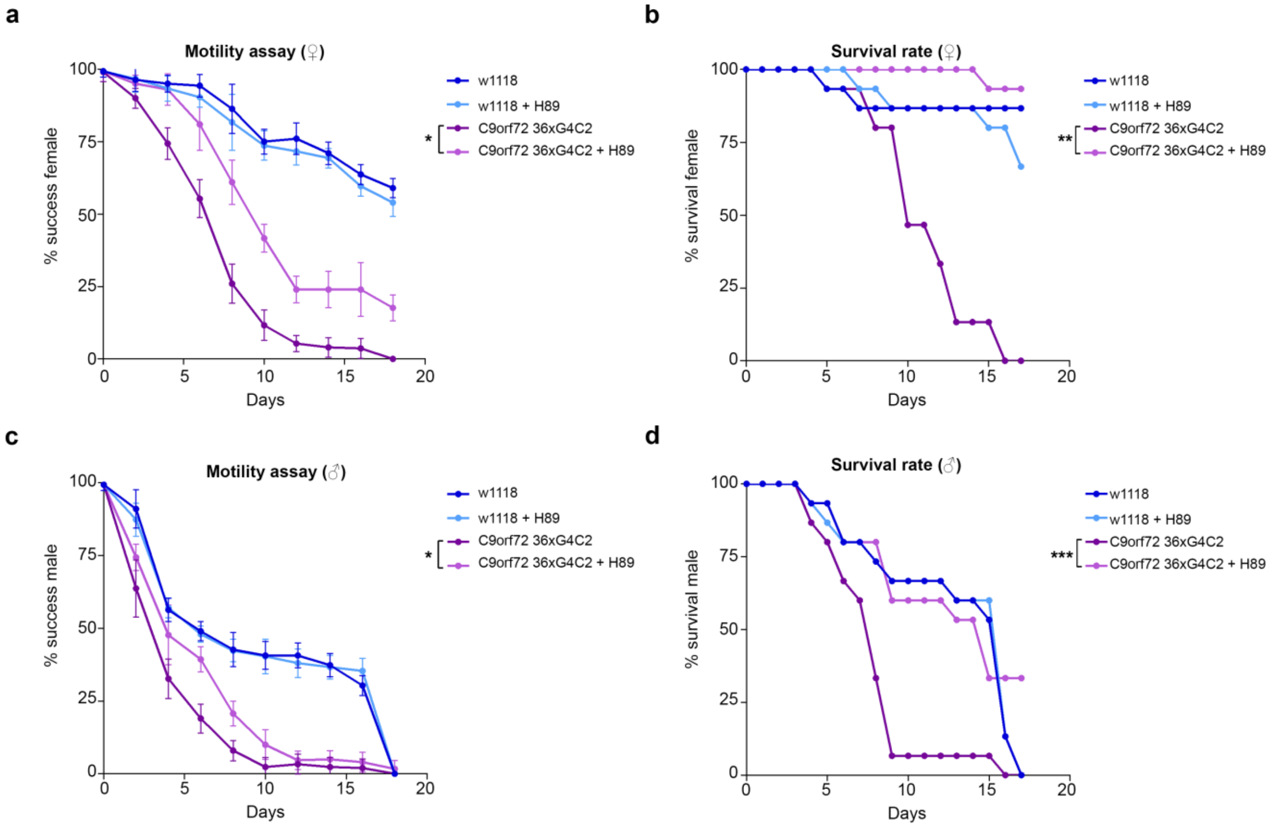

Figure 6 | PKA inhibition through H89 administration improves motility defects and extend lifespan in a *Drosophila* C9orf72 model.

a Graph showing the climbing ability of female flies (♀) carrying the indicated transgenes in neurons using the *elav-gal4* promoter upon treatment with H89 10 µM diluted with 0.1 % of DMSO and 5% sucrose. Data are mean ± SD. 1-way ANOVA followed by Dunnet's multiple comparisons, ****P* 0.0007 C9ORF72 36xG4C2 *versus* C9ORF72 36xG4C2 + H89. **b** Survival curves of female flies (♀) reported in a. Data are mean. 1-way ANOVA followed by Dunnet's multiple comparisons, ***P* 0.0018 C9ORF72 36xG4C2 *versus* C9ORF72 36xG4C2 + H89. **c** Graph showing the climbing ability of male flies (♂) carrying the indicated transgenes in neurons using the *elav-gal4* promoter upon treatment with H89 10 µM diluted with 0.1 % of DMSO and 5% sucrose. Genotypes as in **a**. Data are mean ± SD. 1-way ANOVA followed by Dunnet's multiple comparisons, **P* 0.0215 C9ORF72 36xG4C2 *versus* C9ORF72 36xG4C2 + H89. **d** Survival curves of male flies (♂) reported in **c**. Data are mean. 1-way ANOVA followed by Dunnet's multiple comparisons, ****P* 0.0001 C9ORF72 36xG4C2 *versus* C9ORF72 36xG4C2 + H89.

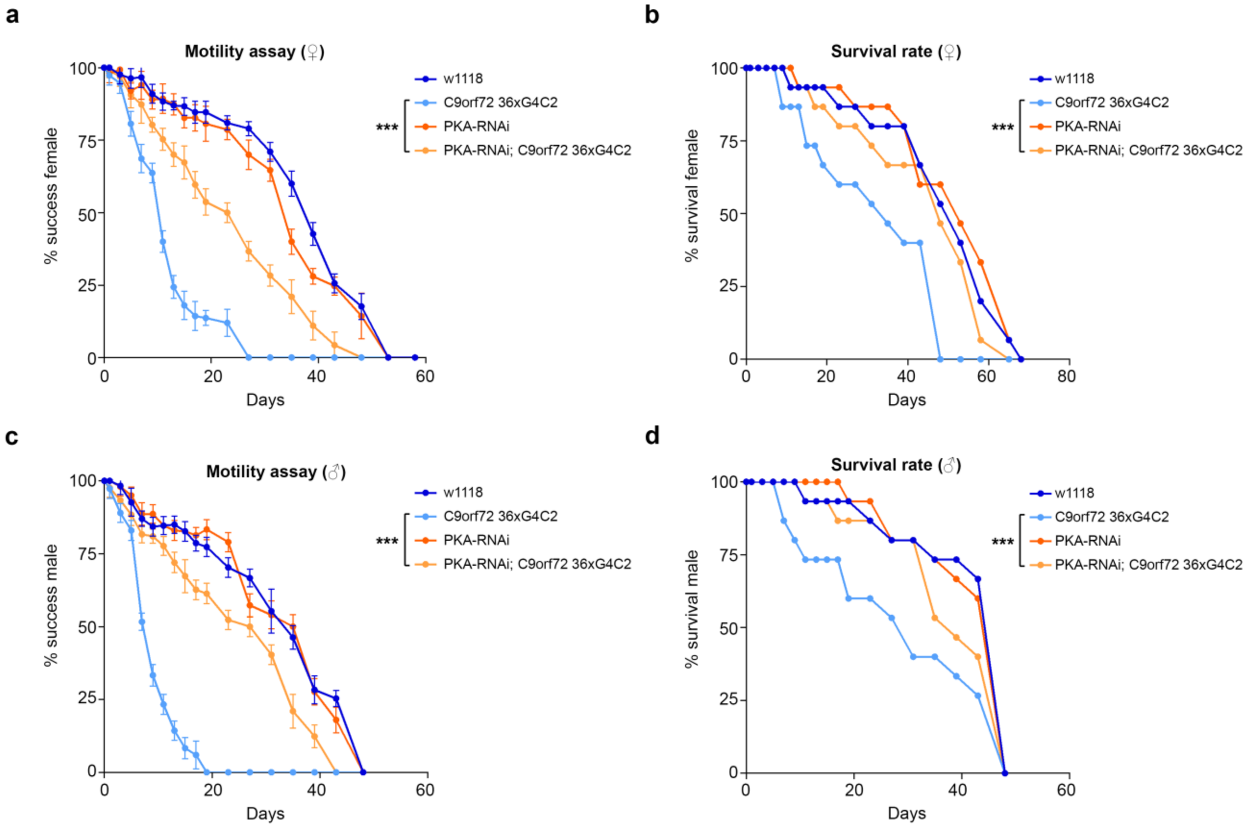

Figure 7 | PKA inhibition through RNAi interference improves motility defects and extend lifespan in a *Drosophila* C9orf72 model.

a Graph showing climbing activity of female flies (♀) co-expressing the *UAS-PKA-RNAi* construct in combination with *UAS C9ORF72 36xG4C2* in neurons using the *elav-gal4* promoter. Data are mean ± SD. 1-way ANOVA followed by Dunnet's multiple comparisons, ****P* 0.0002 C9ORF72 36xG4C2 *versus* PKA-RNAi/ C9ORF72 36xG4C2. **b** Survival curves of female flies (♀) reported in **a**. Data are mean. 1-way ANOVA followed by Dunnet's multiple comparisons, ****P* 0.0001 C9ORF72 36xG4C2 *versus* PKA-RNAi/ C9ORF72 36xG4C2. **c** Graph showing climbing activity of male flies (♂) co-expressing the *UAS-PKA-RNAi* construct in combination with *UAS C9ORF72 36xG4C2* in neurons. Genotypes as in **a**. Data are mean ± SD. 1-way ANOVA followed by Dunnet's multiple comparisons, ****P* 0.0002 C9ORF72 36xG4C2 *versus* PKA-RNAi/ C9ORF72 36xG4C2. **d** Survival curves of male flies (♂) reported in **c**. Data are mean. 1-way ANOVA followed by Dunnet's multiple comparisons, ****P* 0.0001 C9ORF72 36xG4C2 *versus* PKA-RNAi/ C9ORF72 36xG4C2.